University of North Florida
UNF Digital Commons

UNF Graduate Theses and Dissertations | Student Scholarship

2012

Development of a Predictive Model for Bulk-Flow Through A Porous Polymer Membrane Tube

Aaron Robert Meles
University of North Florida

Follow this and additional works at: https://digitalcommons.unf.edu/etd

 Part of the Applied Mechanics Commons

Suggested Citation

Meles, Aaron Robert, "Development of a Predictive Model for Bulk-Flow Through A Porous Polymer Membrane Tube" (2012). *UNF Graduate Theses and Dissertations*. 406.
https://digitalcommons.unf.edu/etd/406

This Master's Thesis is brought to you for free and open access by the Student Scholarship at UNF Digital Commons. It has been accepted for inclusion in UNF Graduate Theses and Dissertations by an authorized administrator of UNF Digital Commons. For more information, please contact Digital Projects.
© 2012 All Rights Reserved

DEVELOPMENT OF A PREDICTIVE MODEL FOR BULK FLOW THROUGH A POROUS POLYMER MEMBRANE TUBE

By

Aaron Robert Meles

A thesis submitted to the School of Engineering
in partial fulfillment of the requirements for the degree of

Master of Science in Mechanical Engineering

UNIVERSITY OF NORTH FLORIDA

COLLEGE OF COMPUTING, ENGINEERING, AND CONSTRUCTION

April, 2012

Unpublished work © Aaron Robert Meles

The thesis of Aaron Robert Meles is approved: (Date)

Signature Deleted

4/4/12

Dr. James Fletcher

Signature Deleted

4/4/12

Dr. Richard Conte

Signature Deleted

4/4/12

Dr. Adel ElSafty

Accepted for the School of Engineering:

Signature Deleted

4/12/12

Dr. Murat Tiryakioglu
Chair

Accepted for the College of Computing, Engineering and Construction:

Signature Deleted

4/14/12

Dr. Mark A. Tumeo
Dean

Accepted for the University:

Signature Deleted

5/2/12

Dr. Len Roberson
Dean of The Graduate School

TABLE OF CONTENTS

LIST OF TABLES

LIST OF FIGURES

LIST OF SYMBOLS, NOMENCLATURE, OR ABBREVIATIONS

A_c Cross-sectional area of the tube

A_s Surface area of the tube

B_0 Geometric constant for mole-based viscous transport equation

c_{ent} Coefficient for pressure loss in the developing region, $\Delta p_z = c_{ent}\rho\overline{u}_i^2/2$

c_f Coefficient of skin friction

d Tube diameter, $d = 2R$

D Pore diameter

J'' Molar flux

K Non-dimensional permeability coefficient, $K = -(dk_D\overline{u}_i^2)/(2\nu^2 t)$

k Darcy's permeability coefficient, gas-specific implementation, $v_w = k\Delta p$

k_D Darcy's permeability coefficient, standard implementation, $v_w = (k_D/(\mu t))\Delta p$

k_M Darcy's permeability coefficient, Mellis et al.'s implementation, $v_w = (k_M/\mu)\Delta p$

l_{pore} Pore length

L Tube length

L_{mod} Tube length modifier, $L_{effective}/L_{actual}$

p Pressure

$\widehat{p}$ Dimensionless pressure, $p/(\rho\overline{u}_i^2/2)$

$\dot{Q}$ Volumetric flow rate

R	Radius of tube
r	Radial direction component
Re_D	Axial Reynolds number in the tube, $\overline{u}_i d/\nu$
Re_R	Axial Reynolds number in the tube, $\overline{u}_i R/\nu$
Re_w	Wall flow parameter, $\overline{v}_w R/\nu$, positive for outflow
t	Thickness of tube wall
u	Axial velocity component
$\widehat{u}$	Dimensionless axial velocity, $u/\overline{u}$
v	Radial direction component
z	Axial direction component
β	Dimensionless axial velocity, $u^2/\overline{u}^2$
Γ	Dimensionless pressure drop, from Kinney's implementation
ϵ	Membrane porosity
η	Dimensionless radial coordinate, $(r/R)^2$
λ_R	Wall flow parameter, $-(v_w R)/\nu$, negative for outflow
λ_D	Wall flow parameter, $-(v_w D)/\nu$, negative for outflow
μ	Dynamic viscosity
ν	Kinematic viscosity
τ	Pore tortuosity

Subscripts and superscripts

i	At the inlet to the porous tube
w	Through the tube wall
ext	Environment outside the porous tube
mem	Membrane
$\overline{}$	Average value
$\widehat{}$	Normalized value
$\dot{}$	Time rate
$''$	Area flux

Abstract of Thesis Presented to the Graduate School
of the University of North Florida in Partial Fulfillment of the
Requirements for the Degree of Master of Science

DEVELOPMENT OF A PREDICTIVE MODEL FOR BULK FLOW THROUGH A POROUS POLYMER MEMBRANE TUBE

By

Aaron Robert Meles

April 2012

Chair: James Fletcher
Major: Mechanical Engineering

While extensive mathematical and numerical work has been done in terms of modeling the mainstream flow in a tube with porous walls, very little has been done experimentally to confirm these various solutions, and what has been done has focused on large sintered metal tubes used in nuclear power applications. Furthermore, these solutions are quite mathematically complex and arduous to implement. In this work, the mainstream flow through a porous polymer membrane tube is examined and a method for calculating the through-membrane flow rate and axial pressure drop is presented. Two membrane tubes are tested experimentally, and a simple set of modeling equations that are physically intuitive are presented which fit the data. A characterization test is described which can be used to determine the permeability coefficient, k_D, for a membrane sample, which can in turn be used to calculate the through-membrane flow rate and axial pressure drop. The models are then evaluated by performing flow-through experiments and measuring the pressures and flows within the membrane. For both membranes tested, the permeability coefficient is determined to be $k_D = 5.9394 \times 10^{-14}$ m^2. For the tube diameters (2 mm and 8 mm) and flow

rates (100-500 sccm) tested, it is shown that for dimensionless tube lengths $\widehat{L} = L/(dRe_D) \geq 0.3$, a model that assumes fully developed flow through the entire tube accurately describes the through-membrane flow rate data. The fully-developed model consistently under-predicts the experimental data for axial pressure drop, therefore it is assumed that the discrepancy is due to an additional pressure loss from the developing region. This loss is determined empirically using the data. The model's validity is examined and compared to that of other authors for the range of flow rates tested.

CHAPTER 1
TOPIC INTRODUCTION

1.1 Motivation

Porous polymer membranes are used for a variety of applications, spanning from distillation of valuable chemicals to water purification. Such membranes are usually created by expanding a polymer sheet in a manner such that pores develop in the originally solid material. If the polymer is made out of a hydrophobic material, such as polytetrafluoroethylene (PTFE), the diameter of the pores can be made small enough that surface tension forces prevent liquids from intruding into the pores, but large enough that gases may still pass. The membrane then prevents liquids from passing while allowing gases to travel through it relatively freely, so long as the operating pressure remains below the capillary pressure needed to force liquid into the pores. Such membranes are used in a process known as membrane distillation, where the more volatile components in a liquid in contact with the membrane's surface will evaporate and pass through the pores to be collected on the opposite side of the membrane. Other applications for polymer membranes include desalination, removing volatile compounds from waste water, and the concentration of valuable compounds in solution (Lawson and Lloyd, 1997).

One potential use for membranes made of hydrophobic materials that has yet to be thoroughly examined is gas-liquid separation. The porous nature of the membrane walls allow gases to escape, while the hydrophobicity of the membrane walls prevents liquids with sufficient surface tension from entering the pores. Given the natural buoyancy of the gas bubbles in such a configuration, a tube-shaped membrane is a practical choice for such an application, as the gas

bubbles would rise to contact the membrane surface no matter the orientation of the tube or the size of the bubbles. Such a membrane would be ideally suited for systems where the gas-liquid separation must occur in a variety of orientations and without any need for a power supply. For instance, portable direct methanol fuel cells, which produce carbon dioxide as a by-product of the anode reaction in the liquid methanol fuel stream, would benefit greatly from such a gas-liquid separation technique. Such a system would require that the membrane tube have a small enough diameter that entrained gas bubbles would contact the tube walls and therefore be able to escape. The tube length must also be large enough that an acceptable amount of gas is vented through the tube walls before the bulk velocity carries the gas out of the porous section. Finally, the pressure head required to move the gas-liquid mixture through the tube must be able to be calculated so that the required amount of pumping energy for the system can be determined.

A wide variety of hydrophobic membranes are available with many differing geometries, material properties, and pore characteristics. However, because both the product and the application are relatively new, very little guidance is provided for aiding in the membrane selection process. Several primary reasons for this exist:

- The membrane pores are microscopic in size and extremely convoluted.
- The distribution of pores and their geometric characteristics are of a random nature.
- The physics of two-phase flow, especially with wall extraction of one of the phases, is complicated and not well understood.
- Such a system is yet to be thoroughly addressed in the literature.

The first two items make it difficult to use manufacturers' specifications (typically defined by features such as porosity and average pore size) to create a predictive

model of flow through the membrane and can only be addressed through experimental membrane characterization. The complication of two-phase flow requires that pure liquid flow and pure gas flow through the tube be understood first, before applying two-phase flow theory to predict the combination of the two. It is the intent of this work to take the first step in this process; that is, to provide an evaluation process for choosing a tubular membrane for a single phase, gaseous application. The work of understanding the liquid phase and its combination with gas into two-phase flow will be left to future research.

This work will therefore address the following:

- The characterization of tubular membrane samples using straight-forward tests to determine useful geometric constants.
- Using these constants to determine the axial pressure drop and the flow rate of the gas vented through the membrane wall.

Through-wall flow rate and axial pressure drop were selected as the parameters of interest as they are necessary to realize the porous tube's effect on a fluid circuit. Therefore, these are the variables necessary for integration of such a tube into a complete system design, as well as providing the necessary information for future work on constructing a model for two phase gas-liquid flow. The results of this analysis will be compared against experimental data to provide insight into the method's accuracy, which will cover the relative lack of literature references.

1.2 Problem definition

In order to provide context and prepare the reader for the literature review presented in Chapter 2, a brief outline of the generic problem statement will be outlined here. The applicable control volumes, coordinate systems, boundary conditions, Navier-Stokes equations, and general membrane flow equations are presented in the following sections. As is shown in Chapter 2, a wide variety of increasingly complex mathematical techniques have been applied to solve the

Navier-Stokes equations for this system, usually with the goal of describing the entire flow field in detail (for instance, the velocities and pressure gradients at every point). In Chapter 3, a new model is presented that instead uses integrated forms of the continuity and momentum equations to model the entire control volume as a whole (using parameters such as total flow through the membrane wall and axial inlet-to-outlet pressure drop). This model is then validated using the experiments detailed in Chapter 4. The results of this series of experiments is presented in Chapter 5, where the accuracy and range of validity of the method are examined. Finally, the suitability of the method for evaluating membrane tubes for use in engineering applications is discussed in Chapter 6.

1.2.1 Flow through the tube

An analytical model of the porous tube must be split into the following two parts:

1. analysis of the flow in an individual pore, which will then be extended to a group of pores over a unit area;
2. analysis of the flow field inside the tube, while recognizing the interaction between the two.

That is, the first analysis will impact the results of the second, as the wall boundary condition will be determined by the flow behavior in the pores. As will be shown, the problem is further complicated by the coupling of the two analyses, as the flow through the pores will be governed by the pressure differential across the pore and the flow through the tube will be governed by the flow through the pores.

Since this study was performed for the specific application of a relatively small direct methanol fuel cell, the range of flow rates will be limited to between 100 and 500 standard cubic centimeters per minute (sccm) of carbon dioxide and to pressures no greater than 10 inH_2O above atmospheric. Finally, this work will focus on analyzing tubes with a constant, circular cross-section.

The nominal properties of the two types of porous tubing used are shown in Table 1-1. As can be seen, the highest Reynolds number for this set of diameters and flow rates is $Re = 644$, and therefore the flow regime will be assumed to be laminar for this analysis.

	TB0302	TB1008
Outer diameter	3 mm	10 mm
Inner diameter	2 mm	8 mm
Porosity	0.6	0.8
Reynolds number Re_D @ 500 sccm	644	161

Table 1-1. Porous tube properties

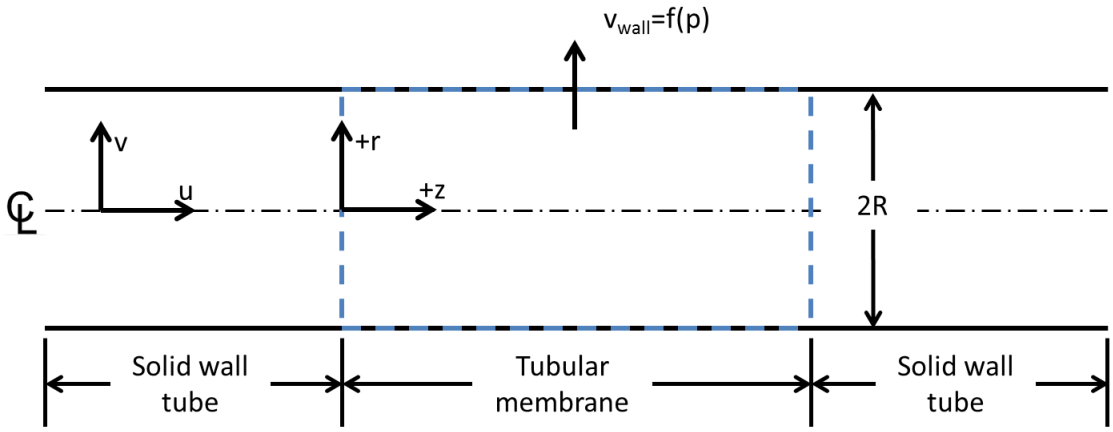

Figure 1-1. Control volume of the tube

The generic control volume typical for an analysis of a porous tube is shown in Figure 1-1. In order to remain consistent with the literature, the velocity component in the z-direction is designated as u and the component in the r-direction is v (note this contrasts with the more common convention of using v_z and v_r, respectively). For the purposes of this analysis, the flow into the membrane tube will be assumed to be fully developed and entering smoothly from a nonporous tube of the same diameter. If a cylindrical coordinate system is used and the flow is assumed to be axisymmetric, the continuity and momentum

equations become:

$$0 = \frac{\partial(rv)}{\partial r} + \frac{\partial(ru)}{\partial z} \tag{1–1}$$

$$\rho\left(v\frac{\partial v}{\partial r} + u\frac{\partial v}{\partial z}\right) = -\frac{\partial p}{\partial r} + \mu\left[\frac{1}{r}\frac{\partial}{\partial r}\left(r\frac{\partial v}{\partial r}\right) + \frac{\partial^2 v}{\partial z^2} - \frac{v}{r^2}\right] \tag{1–2}$$

$$\rho\left(v\frac{\partial u}{\partial r} + u\frac{\partial u}{\partial z}\right) = -\frac{\partial p}{\partial z} + \mu\left[\frac{1}{r}\frac{\partial}{\partial r}\left(r\frac{\partial u}{\partial r}\right) + \frac{\partial^2 u}{\partial z^2}\right] \tag{1–3}$$

The boundary conditions for the problem are:

$$\frac{\partial u(r=0,z)}{\partial r} = v(r=0,z) = u(r=R,z) = 0 \tag{1–4}$$

$$v(r=R,z) = v_w \tag{1–5}$$

where v_w is the velocity in the r-direction at the wall and will be determined by the results of the pore model. In this work, v_w is assumed to be positive for flow leaving the tube, however, the sign convention for v_w as defined by the references may differ and is discussed in Chapter 2. Note that if the wall boundary condition in Equation 1–5 was limited to $v_w = 0$ and the flow was assumed to be fully-developed, the solution to the problem would be the familiar Hagen-Poiseuille equation. While v_w is certainly not zero for the case of a porous wall, the fully-developed assumption needs to be assessed fully and various arguments are presented in the literature review in Chapter 2.

Some physical insight can be gained at this point by rearranging Equation 1–3 to solve for the pressure gradient:

$$\frac{\partial p}{\partial z} = \mu\left[\frac{1}{r}\frac{\partial}{\partial r}\left(r\frac{\partial u}{\partial r}\right) + \frac{\partial^2 u}{\partial z^2}\right] - \rho\left(v\frac{\partial u}{\partial r} + u\frac{\partial u}{\partial z}\right) \tag{1–6}$$

It can be seen in Equation 1–6 that there are two primary contributors to the pressure gradient in the z-direction: viscous effects given by the first term on the right hand side, and momentum transport effects encapsulated in the second term. In Hagen-Poiseuille flow, the second term is zero because the flow is

assumed to be fully-developed, that is, $\partial u/\partial z = 0$. Applying this assumption to the continuity equation 1–1,

$$0 = \frac{\partial (rv)}{\partial r} + 0 \tag{1–7}$$

$$0 = \frac{\partial v}{\partial r} \tag{1–8}$$

Since $\partial v/\partial r = 0$, v is constant for all r. Applying the boundary condition of zero radial velocity at the wall, $v_w = 0$, it can be concluded that v is zero everywhere. Thus, both terms in the second term are zero and the familiar Hagen-Poiseuille problem statement is the result. However, the second term is nonzero when v is not zero at the wall, as is the case with porous walls. Therefore, this additional term will modify the results predicted by the Hagen-Poiseuille equation, as will be shown in Chapter 3.

At this point in the analysis, authors differ in how to best solve Equations 1–1 through 1–3, as is shown in Chapter 2. In Chapter 3, the integrated forms of the continuity and momentum equations are employed to create a model to predict the axial pressure drop and the flow rate through the membrane wall. This model is then evaluated using experimental data in Chapter 5.

Before proceeding, a definition of fully-developed flow for porous tubes is warranted. In typical internal flows, the flow is said to be fully-developed when the axial velocity $u(r, z)$ no longer changes with axial position. That is,

$$\frac{\partial u(r, z)}{\partial z} = 0 \tag{1–9}$$

However, in the case of porous tubes, this relationship will never apply, as the average value of u for a particular cross-section will continue to drop as more fluid is extracted from the tube (much like the bulk temperature will change in a tube with constant heat flux at the walls). Therefore, an approach similar to that used to define a thermal fully-developed condition must be used. Recall that for a flow

to be thermally fully-developed, Equation 1–10 must apply.

$$\frac{d}{dz}\left[\frac{T_w(z) - T(r,x)}{T_w(z) - T_m(z)}\right] = 0 \tag{1–10}$$

where T is the temperature, T_w is the wall surface temperature, and T_m is the mean temperature for a particular cross-section. Replacing the temperature in Equation 1–10 with axial velocity results in:

$$\frac{d}{dz}\left[\frac{u_w(z) - u(r,x)}{u_w(z) - \overline{u}(z)}\right] = 0 \tag{1–11}$$

Applying the no-slip condition, $u_w = 0$, means that Equation 1–11 can be simplified to be in terms of dimensionless axial velocity:

$$\frac{\partial \widehat{u}(r,z)}{\partial z} = 0 \tag{1–12}$$

where $\widehat{u}(r,z)$ is defined as:

$$\widehat{u}(r,z) = \frac{u(r,z)}{\overline{u}(z)} \tag{1–13}$$

where $\overline{u}(z)$ is the mean velocity for a particular cross-section of tube. Therefore, when the dimensionless axial velocity $\widehat{u}$ is no longer changing with axial position, then the flow in the porous tube is fully-developed. This effectively means that the shape of the axial velocity profile is the same for every cross-section.

1.2.2 Flow through the pores

Determination of v_w requires a model for the porous wall itself. While the pores in a porous polymer membrane are in reality a network of highly tortuous passageways of varying area (as shown in the scanning electron microscope image shown in Figure 1-2), it is instructive to first consider a single, simplified, cylindrical pore, such as the one shown in Figure 1-3. What follows is the method for describing pressure-driven flow through a membrane as presented by both Mulder (1996) and Mason and Malinauskas (1983). The diameter of the pore D_{pore} for a porous polymer membrane is typically on the order of microns,

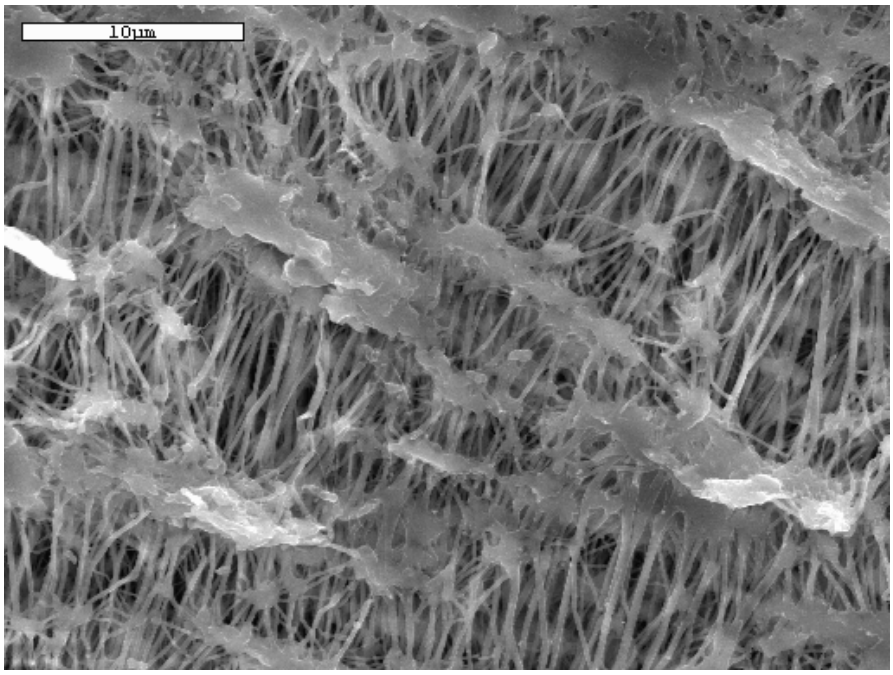

Figure 1-2. Scanning electron microscope image of a porous polymer membrane

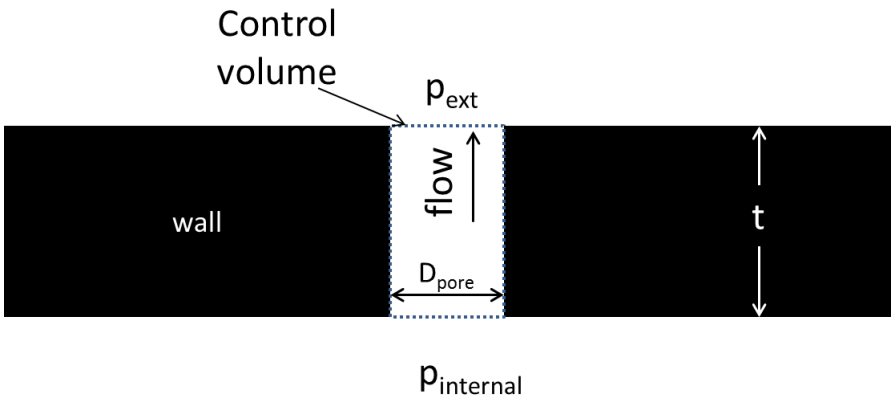

Figure 1-3. Control volume of an individual pore

meaning that the length to diameter ratio of the pore is on the order of 10^3. Assuming, then, that the entrance length effects are negligible and that the flow through the pore is laminar, Hagen-Poiseuille flow exists in the pore and the rate of flow can be calculated using

$$\dot{Q} = \frac{\pi D_{pore}^4 \Delta p}{128 \mu t} \tag{1–14}$$

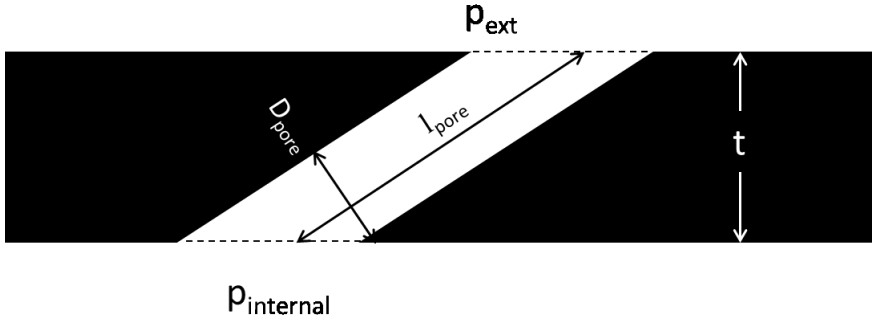

Figure 1-4. Control volume for a tortuous pore

where $\dot{Q}$ is the volumetric flow rate through the pore. It can be seen from Equation 1–14 that for a given pore geometry and gas viscosity, the flow rate through the pore is linearly related to the pressure drop across the pore. Consider now another cylindrical pore, but at an arbitrary angle through the membrane wall, as shown in Figure 1-4. The pore tortuosity, τ, can then be defined as:

$$\tau = \frac{l_{pore}}{t} \tag{1–15}$$

Assuming that the pore tortuosity is known, Equation 1–14 can be modified to be:

$$\dot{Q} = \frac{\pi D_{pore}^4 \Delta p}{128\mu(\tau t)} \tag{1–16}$$

If this pore geometry is then repeated many times over a unit area, the frequency of the pores can be quantified using the porosity, ϵ:

$$\epsilon = \frac{A_{pores}}{A_{total}} \tag{1–17}$$

Assuming that the porosity of a given membrane is constant, Equation 1–16 can be rewritten in terms of volumetric flux Q'' and porosity as:

$$Q'' = \frac{\epsilon D_{pore}^2 \Delta p}{32\mu(\tau t)} \tag{1–18}$$

and hence knowledge of the pore size, tortuosity, membrane thickness, and pressure differential will provide the flow rate through the porous media. In reality, however, pore sizes, porosity, and tortuosity are typically not constant over the entire membrane area, nor are the pores straight or cylindrical as shown in Figure 1-4. Thus, determining the pore geometry can best be achieved via careful experimentation. This is easily accomplished by grouping the geometric terms in Equation 1–18 into a single term, resulting in Darcy's Law for porous media:

$$Q'' = \frac{k_D \Delta p}{\mu t} \tag{1–19}$$

where k_D is the permeability coefficient, which is determined via experiment and accommodates the impact of these terms. (Note that $Q'' = \dot{Q}/A_s$, the volumetric flux, is equivalent to v_w.) As with the model for the single pore, pressure and flow rate are expected to have a linear relationship for a given gas and membrane. Determination of k_D is discussed in further detail in Chapter 4. For now it is enough to note that the flow rate of gas through the porous media is dependent on the pressure differential across the membrane. This will couple together the membrane problem in Equation 1–19 and the tube problem in Equations 1–1 through 1–5.

CHAPTER 2
LITERATURE REVIEW

2.1 Flow through a pipe with suction

2.1.1 Fully developed flow with constant wall velocity

Early work on understanding laminar flow through a tube with porous walls focused on finding perturbation solutions to Hagen-Poiseuille flow by assuming that the velocity of the flow through the porous wall was constant and that the flow field was fully-developed (as explained on page 7). Important early work on flow through a porous tube was done by Yuan and Finkelstein (1956), which started with the Navier-Stokes equations in cylindrical coordinates (shown in Figure 1-1) and assumed that the radial velocity of the fluid flow through the porous wall v_w was constant for all z. Assuming two-dimensional, incompressible flow, the authors' stream function is

$$ru = \frac{\partial \psi}{\partial r} \tag{2–1}$$

$$-rv = \frac{\partial \psi}{\partial z} \tag{2–2}$$

which satisfies the continuity equation automatically. For the boundary conditions given in Equation 1–4 and $v(r = R, z) = v_w = constant$, as assumed above, the stream function was transformed to:

$$\psi = \frac{R^2}{2}\left[\frac{u_i}{f'(0)} + 4v_w\frac{z}{R}\right] f(\eta) \tag{2–3}$$

where $\eta = (r/R)^2$. By inserting Equation 2–3 into Equations 2–1 and 2–2, the authors developed expressions for the velocity components:

$$\begin{aligned} u &= u_i \left[\frac{1}{f'(0)} + 4 \frac{\lambda_R}{Re_R} \frac{z}{R} \right] f'(\eta) \\ v &= -2 v_w \frac{f(\eta)}{\sqrt{\eta}} \end{aligned} \tag{2–4}$$

where Re_R is the axial Reynolds number at the inlet to the porous tube, $Re_R = u_i R/\nu$, and λ_R is the wall flow parameter, defined as $\lambda_R = -v_w R/\nu$, where positive values of λ_R correspond to flow being injected into the tube and negative values correspond to outflow from the tube. The authors then inserted these values into the Navier-Stokes equation, differentiated with respect to η and integrated the resulting expression to yield:

$$\eta f''' + f'' - \lambda_R \left(f'^2 - f f'' \right) = c \tag{2–5}$$

for $\lambda_R \leq 1$, and

$$f'^2 - f f'' - \frac{1}{\lambda_R} \left(\eta f''' + f'' \right) = k \tag{2–6}$$

for $\lambda_R > 1$, where c and k are constants of integration. The boundary conditions were transformed to:

$$\begin{aligned} f(0) = f'(1) &= 0 \\ \lim_{\eta \to 0} f''(\eta) &= 0 \\ f(1) &= \frac{1}{2} \end{aligned} \tag{2–7}$$

The authors then determined a solution for small λ_R by developing a power series around $\lambda_R = 0$:

$$f = f_0 + \lambda_R f_1 + \lambda_R^2 f_2 + ... + \lambda_R^n f_n \tag{2–8}$$

$$c = c_0 + \lambda_R c_1 + \lambda_R^2 c_2 + ... + \lambda_R^n c_n \tag{2–9}$$

By substituting this into Equation 2–5 and solving with the boundary conditions in Equation 2–7, authors' expression for $f(\eta)$ was:

$$\begin{aligned} f(\eta) = & \left(\eta - \frac{1}{2}\eta^2\right) + \lambda_R \left(-\frac{\eta}{18} + \frac{\eta^2}{8} - \frac{\eta^3}{12} + \frac{\eta^4}{72}\right) + \\ & \lambda_R^2 \left(\frac{83}{5400}\eta - \frac{19}{540}\eta^2 + \frac{11}{432}\eta^3 - \frac{1}{144}\eta^4 + \frac{1}{720}\eta^5 - \frac{1}{10800}\eta^6\right) \end{aligned} \tag{2–10}$$

$$c = -1 - \frac{3}{4}\lambda_R + \frac{11}{270}\lambda_R^2 \tag{2–11}$$

These were then used in conjunction with Equation 2–4 to determine the velocities:

$$\begin{aligned} \frac{u}{u_i} = & \left[\frac{1}{1 - \frac{\lambda_R}{18} + \frac{83}{5400}\lambda_R^2} + 4\frac{\lambda_R}{Re}\frac{z}{R}\right] \times \\ & \left[1 - \eta + \frac{\lambda_R}{36}(-2 + 9\eta - 9\eta^2 + 2\eta^3)\right. \\ & \left. + \frac{\lambda_R^2}{10800}(166 - 760\eta + 825\eta^2 - 300\eta^3 + 75\eta^4 - 6\eta^5)\right] \end{aligned} \tag{2–12}$$

$$\begin{aligned} \frac{v}{u_i} = & -\frac{2\lambda_R}{Re\sqrt{\eta)}}\left[\eta - \frac{1}{2}\eta^2 + \frac{\lambda_R}{72}(-4\eta + 9\eta^2 - 6\eta^3 + \eta^4)\right. \\ & \left. + \frac{\lambda_R^2}{10800}(166\eta - 380\eta^2 + 275\eta^3 - 75\eta^4 + 15\eta^5 - \eta^6)\right] \end{aligned} \tag{2–13}$$

These results were then applied to the Navier-Stokes equation to find the pressure distribution:

$$\frac{p(0,r) - p(z,r)}{\frac{\rho u_i^2}{2}} = \frac{8}{Re}\left[1 + \frac{3}{4}\lambda_R - \frac{11}{270}\lambda_R^2\right]\left[\frac{1}{f'(0)} + 2\frac{\lambda_R}{Re}\frac{z}{R}\right]\left(\frac{z}{R}\right) \tag{2–14}$$

where ρ is the fluid density. A solution for large λ_R is also presented by the authors by developing a power series around $1/\lambda_R = 0$, however it is not included here because such high suction rates are outside the scope of this work.

Using these results, axial pressure drop can be predicted by choosing a value for the wall velocity v_w and calculating the corresponding value of λ_R. A plot of axial pressure drop for various λ_R for this solution method is shown in

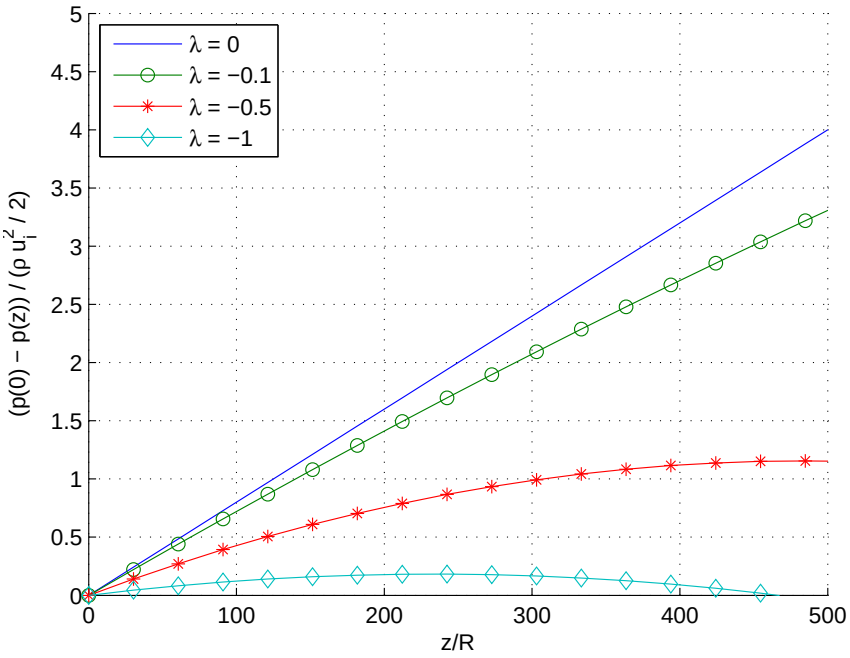

Figure 2-1. Axial pressure drop for various λ_R using Yuan's method, $Re = 1000$

Figure 2-1. While the assumption of constant wall velocity over the entire length of the tube is non-physical in most cases, this solution can be instructive as to what the general trend will be in reality. As can be seen, increasing wall outflow velocity (corresponding to increasingly negative values of λ_R) results in lower overall pressure drop for a given length of tubing. This intuitively makes sense: as λ_R increases in magnitude, more flow is extracted from the bulk flow through the tube walls, slowing the velocity (as shown in Figure 2-2) of the flow and causing some of the dynamic pressure head to be recovered into static pressure. Thus, for any amount of wall outflow, the pressure drop is expected to be lower than the pressure drop predicted by the Hagen-Poiseuille equation (i.e., for $\lambda_R = 0$).

This perturbation solution has been adapted for a variety of channel geometries, producing very similar results: for flow in circular ducts by Terrill and Thomas (1969), Bansal (1966), and White Jr (1962); for flow in a rectangular slot by Berman (1953), Yuan (1956), and Verma and Bansal (1966); for an annulus by Berman (1958b) and Chatterjee and Belfort (1986); and for arrays

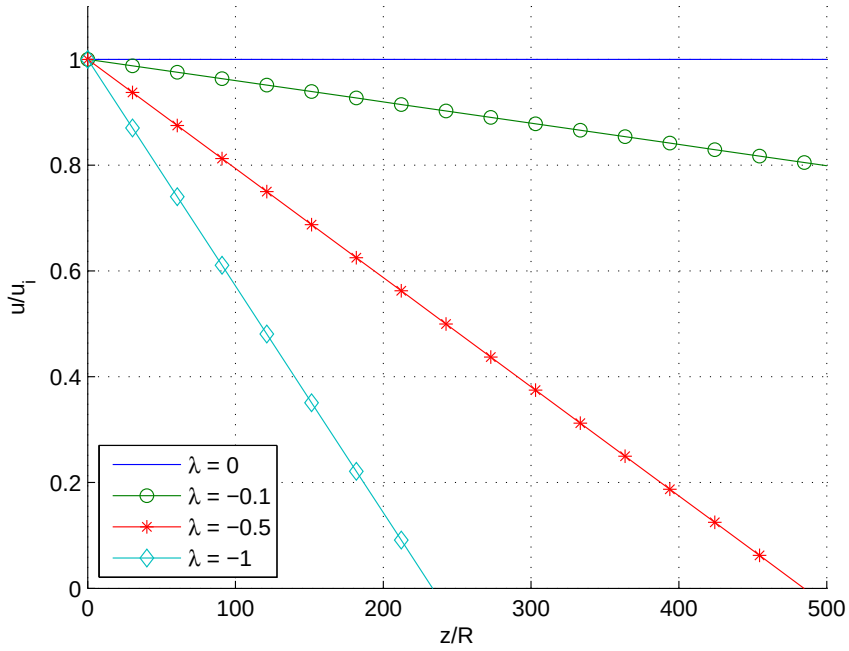

Figure 2-2. Axial centerline velocity for various λ_R using Yuan's method, $Re = 1000$

of tubes by Moussy and Snider (2009). Berman (1956) attempted to evaluate the validity of these solutions by comparing them to the results of a numerical integration technique, and concluded that the solution of Yuan and Finkelstein (1956) was valid for all λ_R except for large outflow values. The solution of Sellars (1955) was proposed as a more accurate alternative for large outflow values, who developed a power series solution at $\lambda_R \to -\infty$. Note that, in all cases, the proposed solutions were not validated with experimental data; any evaluation of the solution was done by comparing to numerical solutions that were assumed to be accurate, as was the case with Berman (1958a).

Further work was done using the solutions presented by Berman and Yuan and Finkelstein as a starting point, typically attempting to extend the range of λ_R for which the solution was applicable. Morduchow (1957) used the method of averages to produce a single average solution which was applicable for all positive λ_R (injection). By placing the condition that the differential equation

2–5 be satisfied on average for all r, that is, that the axial pressure gradient is constant for all points in any given cross section of tube, the author determined a solution by assuming a polynomial solution for f, resulting in:

$$F(\eta) = \left(\eta - \frac{\eta^2}{2}\right) + a_3(\eta - 2\eta^2 + \eta^3) + a_4(2\eta - 3\eta^2 + \eta^4) \tag{2–15}$$

$$\begin{aligned} a_3 &= b a_4 \\ 0 &= (b+2)^2 Re_w a_4^2 - c a_4 + \frac{Re_w}{2} \\ b &= -4\frac{6 - Re_w}{4 - Re_w} \\ c &= 12(3+b) - Re_w(7+3b) \end{aligned} \tag{2–16}$$

where $Re_w = v_w R/\nu$, which is differentiated here from λ_R because Re_w is positive for outflow, whereas λ_R is negative for outflow. The advantage of this method of solution is that a solution can be determined for a wide range of Re_w, rather than the small value or large value approximations made by Yuan and Finkelstein. Morduchow only presents a solution for injection by solving Equation 2–16 for negative Re_w, however a similar set of expressions can be derived for positive Re_w using the same method.

This class of solutions, also referred to as “similarity” solutions because the velocity profiles are similar for all cross-sections due to the fully-developed assumption, is examined in a review by Berman (1958a), who compared the similarity solutions previously discussed here to numerical solutions. The review concluded that the mathematics of this formulation of the problem dictated that there is no similarity solution for $2.3 < Re_w < 9$ and that the solutions for $Re_w > 9$ were of dubious physical significance, as each of the possible solutions contain nonphysical features, such as inflection points in the velocity. In addition, several of these high Re_w solutions exhibit reverse flow in portions of the flow profile, which would likely result in flow separation and possibly turbulence, meaning

that the original assumption of laminar flow is not valid. Berman also concluded that the averaging method of Morduchow was accurate for all injection values of λ_R and even some low suction values, but began to deviate from the numerical solutions when $\lambda_R < -4$.

The first experimental data published was that of Bundy and Weissberg (1970), who constructed a 3m long porous titanium tube with a 35mm inner diameter and injected air through the porous walls. Pressure drop and axial velocity measurements were taken and compared to the solution of Berman (1958a) for $0 \leq \lambda_R \leq 8$. The pressure results were presented in terms of a K parameter, defined as:

$$K = \frac{2\rho R^2 \Delta p}{\mu^2 X} \tag{2–17}$$

$$X = \left(\frac{z_2}{R} - \frac{z_1}{R}\right)\left[Re - \left(\frac{z_2}{R} + \frac{z_1}{R}\right)\lambda_R\right] \tag{2–18}$$

The authors' plot of K versus λ_R was quite linear for $0 < \lambda_R < 10$, and the data gathered for $0 < Re_R < 508$ in this region matches the fully-developed solution of Berman (1958a) well in the last 1.83m of tube, leading to the conclusion that the flow was fully developed for that region. Bundy and Weissberg did not collect any data for outflow and did not present data from the developing region.

Belfort and Nagata (1985) also published experimental data for a 30 cm long stainless steel tube with an inner diameter of 2 cm. Water was used as the fluid and flow rates of $500 < Re_R < 50000$ and $0 \leq Re_w \leq 2$ were tested. It was empirically determined that the transition to turbulence was shifted from the classical value of $Re_R = 2100$ for a nonporous tube to $Re_R = 4000$ for the porous tube examined. The results were plotted in terms of skin friction coefficient c_f versus Re_R and Re_w, however, no comparisons were made to theoretical predictions. The validity of the no-slip condition on the membrane wall was also discussed and it was determined that while, in general, it is not appropriate for

porous walls, in the typical operating range used with polymer membranes (low Re_R and Re_w), the no-slip condition was deemed to be a valid approximation.

Kinney (1968) used the same method presented by Yuan and Finkelstein (1956), assuming fully developed flow with constant wall velocity, but instead cast the momentum equation in terms of a dimensionless axial pressure gradient, Γ:

$$\eta f''' + f'' - \frac{\lambda_D}{2}(f'^2 - ff'') + \frac{\Gamma}{16} = 0 \tag{2–19}$$

$$\Gamma = -\frac{Re_D}{\rho \overline{u}^2}\frac{\partial p}{\partial \xi} \tag{2–20}$$

$$\xi = x/R \tag{2–21}$$

noting that here, the Reynolds number uses the tube diameter as the length scale, $Re_D = 2Re_R = \overline{u}d/\nu$ and $\lambda_D = 2\lambda_R = \overline{v}_w d/\nu$. Through additional manipulation (a portion of which is detailed in Appendix B), the author shows that Γ is equivalent to the addition of two contributing components: wall friction effects and axial momentum flux (recall a similar discussion regarding Equation 1–6):

$$\Gamma = c_f Re_D + 4\beta\lambda_D \tag{2–22}$$

$$\beta = \frac{u^2}{\overline{u}^2} \tag{2–23}$$

where c_f is the coefficient of wall friction and $\lambda_D = -v_w d/\nu$. As can be seen, the first term in 2–22 is the effect of wall friction, while the second is that of changing momentum flux. Kinney employed a numerical solution to solve Equation 2–19 and the subsequent contribution of each effect to the total pressure drop, ultimately arriving at similar quantitative conclusions as Yuan and Finkelstein (1956). A solution for the temperature profile was also presented.

Extending Kinney's results, Raithby (1971) fit an empirical equation to relate $c_f Re$ to λ_D:

$$c_f Re_D = \left(0.0481 + \frac{0.0494}{(\lambda_D + 4.70)^{0.800}}\right)^{-1} \tag{2–24}$$

Raithby also concluded that as λ_D decreases to the critical point of $\lambda_D = -4.5978$, the wall velocity gradient decreases to zero, beyond which a second solution is found where back flow occurs at the wall. However, he concluded that such a profile would be unlikely, since the high pressure gradient accompanying it would likely trip the flow into turbulence.

2.1.2 Fully developed flow with variable wall velocity

Various solutions for fully developed flow with variable wall velocity have been determined, differing chiefly in the way in which the variable wall velocity is treated. Terrill (1982) solves the problem using the stream function in Equations 2–1 and 2–2 and assuming the solution is of the form:

$$\psi = f_0(\eta) + \sum_{i=1}^{\infty} e^{\alpha_i z_i} f_i(\eta), \quad \alpha_i \neq 0 \tag{2–25}$$

While mathematically interesting, the final solution is of little practical use, as it requires that either the u or v velocity field is known a priori. A similar approach was presented by Terrill (1983) by assuming that the solution was of the form:

$$u = u_0(r) + \frac{\partial}{\partial z}\phi(r, z) \tag{2–26}$$

$$v = \frac{\partial \phi}{\partial r}(r, z) \tag{2–27}$$

where $u_0(r)$ is the velocity component from the Hagen-Poiseuille solution. This method also required foreknowledge of the u or v velocity profile in order to formulate the solution.

The work of Mellis et al. (1993) introduced a pair of similarity solutions for porous tube flows depending on whether v_w was constant or pressure dependent. It was first assumed that the solution was of the form:

$$u = \overline{u}(z) f'(\eta) \tag{2–28}$$

where $\eta = (r/R)^2$. By assuming that Re_w is small, the authors manipulated this into the following expression for the pressure distribution:

$$\frac{dp}{dz} = -\frac{8\mu\overline{u}}{R^2}(1 - \frac{3}{4}Re_w) \tag{2–29}$$

This expression was then solved in two ways: (1) assuming a constant wall velocity, which allows retention of the inertial term $(1 - 3/4Re_w)$, or (2) assuming a pressure-dependent wall velocity, which requires assuming that $(1 - 3/4Re_w)$, which the authors call an inertial term, is negligible (which is claimed to be appropriate when Re_w is small). The pressure-dependent solution is:

$$\frac{p(0) - p(L)}{\frac{\rho u_i^2}{2}} = \frac{64}{Re\frac{2R}{L}}\left(\frac{\sinh k_M^*}{k_M^*} - \frac{(\cosh k_M^* - 1)^2}{k_M^* \sinh k_M^*} - \frac{8Re_w(\cosh k_M^* - 1)}{Re\frac{2R}{L}k_M^* \sinh k_M^*}\right) \tag{2–30}$$

$$k_M^* = \frac{4L}{R}\sqrt{\frac{k_M}{R}} \tag{2–31}$$

where k_M is a thickness-inclusive form of Darcy's permeability coefficient, $v_w = k_M \Delta p/\mu$. These model predictions were compared against an experiment using water flow through a porous steel tube. The experimental data showed that in every tested case, the model under predicted the experimental axial pressure drop. The deviation between experiment and theory did not trend with Re_w, meaning that no range of Re_w for which the method is applicable was determined. In fact, it was concluded that for low outflow values ($Re_w \leq 0.25$), a constant wall flux model was more accurate in predicting experimental results. An examination of the data also resulted in the conclusion that wall outflow had the greatest effect on the flow field at $1,000 < Re_R < 15,000$. It was also concluded that for $Re_R < 1,000$ and $Re_w \leq 0.25$, wall outflow had a minimal effect on pressure drop. Experimental data was also collected in the transitional and turbulent regime, however no model was introduced to describe these flows.

Also assuming a pressure-dependent wall velocity, Karode (2001) developed a solution by breaking up the tube into a number of infinitesimally small segments. A solution for axial pressure drop was determined by modifying the Hagen-Poiseuille equation by removing $\dot{Q}_{mem} = v_w A_{mem}$ amount of fluid in each segment and integrating over the tube length:

$$\Delta P = \frac{1}{2}\frac{8\mu\dot{Q}_i}{\pi R^4 \Lambda}\left(e^{\Lambda z} - e^{-\Lambda z}\right) + (P_i - P_{ext})\left(1 - \frac{e^{\Lambda z} - e^{-\Lambda z}}{2}\right) \tag{2–32}$$

$$\Lambda = \sqrt{\frac{16\mu k}{R^3}} \tag{2–33}$$

where $\dot{Q}_i$ is the inlet flow rate, P_i is the inlet pressure, P_{ext} is the permeate pressure, and k is the membrane permeability. This equation was compared to the results of a CFD simulation, and the results of Equation 2–32 were within 2-10% of the CFD results, which was shown to be an improvement over the models introduced by Berman (1953) and Yuan and Finkelstein (1956).

Munson-McGee (2002) developed a solution with a similar form to that of Karode, but simplified the problem by assuming that the axial pressure profile could be approximated by a quadratic and fit the coefficients using boundary conditions, resulting in:

$$p(z) = a + bz + cz^2 \tag{2–34}$$

$$a = p_i = p(z = 0) \tag{2–35}$$

$$b = -\frac{4\mu^2}{\rho R^3} Re_R \tag{2–36}$$

$$c = \frac{24\mu k}{\rho R^3}\left[\frac{(p_i - p_{ext})\rho R^3 - 2\mu^2 L Re_R}{3R^3 - 8\mu k L^2}\right] \tag{2–37}$$

The velocities could then be expressed in terms of these coefficients:

$$u(r,z) = -\frac{\mu Re_R}{\rho R}\left(1 - \frac{4k\rho}{\mu Re_R}\left[(p_i - p_{ext})z + \frac{bz^2}{2} + \frac{cz^3}{3}\right]\right)\left[1 - \left(\frac{r}{R}\right)^2\right] \tag{2–38}$$

$$v(r,z) = k\left[(p_i - p_{ext}) + bz + cz^2\right]\left[2\left(\frac{r}{R}\right) - \left(\frac{r}{R}\right)^3\right] \tag{2–39}$$

This solution was compared to the results of a finite element model for several specific cases, which were:

1. $p_i = p_{i,min}$, which is the inlet pressure necessary so that $p(z = L) = p_{ext}$.
2. $p_i = p_{i,max}$, such that $u(z = L) = 0$, in other words, all of the fluid escapes through the membrane wall.
3. $p_i = p_{median}$, the inlet pressure halfway between p_i, min and p_i, max.

The author determined that the finite element model and the model laid out in Equations 2–34 through 2–39 matched to within 0.5% in all examined cases.

While the theoretical work on solving fully-developed flows with uniform wall suction or injection has largely been completed, further work continues to be accomplished, mostly in the realm of oscillatory flow. For example, oscillatory tube flow is studied for large and small values of injection and suction by Skalak and Wang (1977). Majdalani and Flandro (2002) also developed a solution for oscillatory flow in pipes with a uniform wall velocity, although this was limited to injection and not outflow.

2.1.3 Developing flow

While the early work done on this topic focused on solutions that assumed a fully-developed profile, the next generation of work would attempt to create a solution for a developing flow profile. One of the first approaches to this problem was taken by Weissberg (1959), who used the same method of averages employed by Morduchow (1957) to describe the flow field in the developing region in addition to the fully developed region. The solution assumed that the wall velocity was constant and the inlet velocity profile could be represented by a polynomial — in this case, the Hagen-Poiseuille parabola. The author defined a dimensionless z-coordinate as $\zeta \equiv 1 - (2Re_w/Re_R)(x/R)$ and the stream function

ψ as:

$$\begin{aligned} \frac{\partial \psi}{\partial r} &= ru \\ -\frac{\partial \psi}{\partial x} &= rv \end{aligned} \tag{2–40}$$

and a "dimensionless stream function" F as:

$$F(\zeta, \eta) \equiv \frac{\psi(x, r)}{\psi(x, R)} \tag{2–41}$$

The Navier-Stokes equation were then simplified to:

$$Re_w \left[FF_{\eta\eta} - F_\eta^2 + \zeta(F_\zeta F_{\eta\eta} - F_{\zeta\eta} F_\eta) \right]_\eta - 2(\eta F_{\eta\eta})_{\eta\eta} = 0 \tag{2–42}$$

where a ζ or η subscript indicates differentiation with respect to the subscripted variable. The author noted that in the case of fully-developed flow discussed in the previous section, all derivatives with respect to ζ would be zero and Equation 2–42 would reduce to that of Morduchow, with the slight exception that Morduchow's $f = F/2$. The author then integrated this over η, which resulted in a differential equation equivalent to Equation 2–15, but in this case the constants a_3 and a_4 were functions of ζ. The constants were determined to be:

$$a_3 = b a_4 \tag{2–43}$$

$$b = -4 \frac{6 - Re_w}{4 - Re_w} \tag{2–44}$$

$$c = 10 Re_w - 72 \tag{2–45}$$

a_4 was determined from solving the differential equation

$$Re_w \left[2(b+2) + (b+2)^2 a_4 \right] \zeta \frac{da_4}{d\zeta} + A(a_4) = 0 \tag{2–46}$$

where

$$A(a_4) = 2Re_w - c a_4 + Re_w (b+2)^2 a_4^2 \tag{2–47}$$

This solution, when extended to sufficiently high ζ, matches that of Morduchow, meaning that for a tube with sufficient length for fully developed flow to occur, the similarity solutions from the previous section are valid for the fully developed region. Furthermore, it gives insight into the phenomenon noted by Berman (1958a) where no similarity solution exists for $2.3 < Re_w < 9$: for these outflow rates, the axial velocity drops to zero before the end of the entrance region. Physically, this means that all of the flow has been removed via outflow prior to the flow becoming fully developed. Thus, the mathematical anomaly originally discovered by Berman is explained by including an entrance region to the solution formulation. It can then be concluded that similarity solutions do not hold for flow with $Re_w > 2.3$, as the fully developed condition that is assumed for the similarity solutions is never present in the tube.

Brady (1984) also studied the developing region for a constant wall velocity, calculating a numerical solution using a finite difference and time marching scheme to solve the boundary layer equations for internal flow. Although the author used a different solution method, similar conclusions were drawn to those of Weissberg, namely that similarity solutions closely matched the developing flow solution for most of the tube length when $Re_w < 2.3$. It was also determined that for for sufficiently large Re_w ($Re_w \geq 25$), the similarity solution again becomes an adequate approximation, assuming that the inlet profile is itself a similarity solution.

The solution of Hornbeck et al. (1963) allowed for variable, pressure driven wall velocity by using the following non-dimensional variables:

$$Z = \frac{\nu z}{R^2 \overline{u}_i} \tag{2–48}$$

$$R = \frac{r}{R} \tag{2–49}$$

$$U = \frac{u}{\overline{u}_i} \tag{2–50}$$

$$V = \frac{vR}{\nu} \tag{2–51}$$

$$P = \frac{p - p_{ext}}{\rho \overline{u}_i^2} \tag{2–52}$$

$$A = \frac{R k_D \overline{u}_i^2}{\nu^2 t} \tag{2–53}$$

where k_D is the Darcy permeability coefficient such that $v_w = (k_D/\mu t)(p - p_i)$. Using these non-dimensional variables, the author cast the Navier-Stokes equations in the following form:

$$U\frac{\partial U}{\partial Z} + V\frac{\partial U}{\partial R} = -\frac{\partial P}{\partial Z} + \frac{\partial^2 U}{\partial R^2} + \frac{1}{R}\frac{\partial U}{\partial R} \tag{2–54}$$

$$R\frac{\partial U}{\partial Z} + \frac{\partial}{\partial R}(VR) = 0 \tag{2–55}$$

A finite difference scheme was then employed to solve these equations. Cases using two different inlet velocity profiles (uniform and parabolic) and two different wall conditions (constant v_w and pressure-driven v_w) were evaluated. The parabolic inlet with constant v_w case is compared to the solution of Weissberg and the results agreed very closely. Other cases were run with varying degrees of v_w and inlet velocity, and it was determined that it was possible to either have an increasing or decreasing pressure gradient, depending on the value of v_w and the shape of the inlet profile. In general, it was shown that parabolic inlet profiles tended to result in a pressure rise as flow traveled down the tube, as the velocity gradient at the wall was low enough that the momentum loss due to wall outflow dominated the wall friction effects. The opposite was true for a uniform inlet profile. It was also illustrated that for low inlet pressures and high wall permeabilities, the solution approached that of the constant wall velocity solution. Finally, an examination of entrance lengths showed that for wall suction, the entrance length for a parabolic inlet velocity profile was much shorter than for a uniform velocity profile.

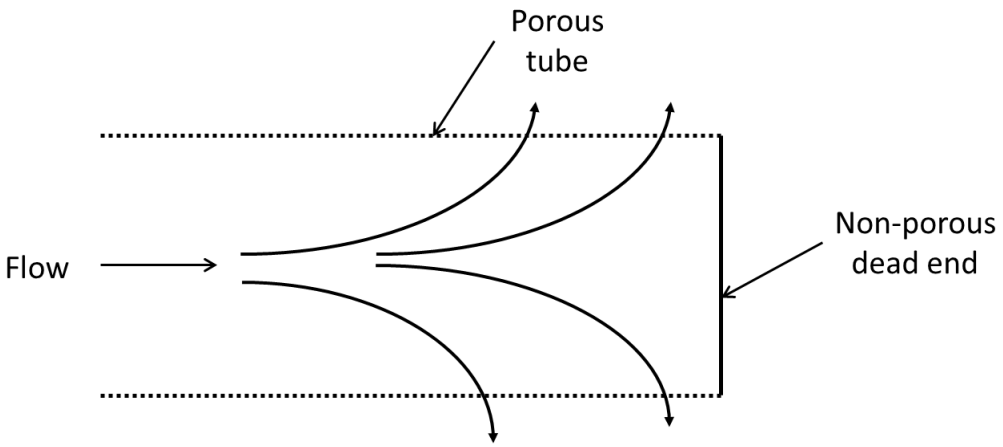

Figure 2-3. Dead-ended tube

As can be seen, all of the solutions for developing flow to this point have required numerical solutions. As the purpose of this work is to provide a practical method for evaluating membranes for engineering design, a numerical solution will not be pursued here. However, it should be noted that if model fidelity in the developing region is a desired characteristic, the state of the art indicates that a numerical solution is necessary.

2.1.4 Flow in dead-ended tubes

Quaile and Levy (1972), Quaile and Levy (1975) and Galowin et al. (1973) studied the flow profile in dead-ended heat pipes, as illustrated in Figure 2-3, rather than open-ended tubes. Quaile and Levy (1972) collected an data from an experiment that flowed silicone fluid through a sintered porous pipe for $2.21 \leq Re_w \leq 5.02$. It was shown that similarity solutions, such as that of Yuan and Finkelstein (1956), did not agree well with the data, while developing flow solutions, such as those of Weissberg (1959) and Hornbeck et al. (1963), were quite accurate when compared to the data. In another look at dead-ended porous pipe data, Quaile and Levy developed a theoretical solution by assuming a constant v_w and solving the dimensionless stream function from Equation 2–41

by expanding a power series in η:

$$F(\xi,\eta) = \sum_{i=1}^{N} a_i(\xi)\eta^{2i} \tag{2–56}$$

where in this case $\eta = r/a$, $\xi = x/L$, and a_i are undetermined coefficients to be solved for. The model was compared to an expanded experimental data set, and the model fit the data fit well for the range of injection Re_w tested, $0 < Re_w < 16$. It was also shown that, for $Re_w < 1.0$, the predicted pressure drop matched that of the similarity solutions quite closely, however no data was taken in this region.

Like Quaile and Levy, Galowin et al. (1973) studied a dead-ended porous tube, but instead allowed for a variable v_w by employing Darcy's Law. The method eschewed the use of a stream function and instead non-dimensionalized the problem and solved it numerically. Key to the solution was the assumption of a quadratic velocity profile of the form:

$$\frac{u}{u_i} = [1 + f(z)](1 - r^2) \tag{2–57}$$

where the function $f(z)$ represents the change in the velocity profile from the Hagen-Poiseuille inlet profile as the flow moves through the tube. The results of method were then compared against the dead-ended tube experimental data collected by Quaile and Levy (1972), and good agreement was found between the theory and data. Again, the mismatch between the similarity solution and data was highlighted.

Terrill (1983), whose approach was discussed in the previous section, also discussed the specific case of a closed-ended tube, developed the following relationship:

$$\frac{p(L) - p(0)}{\frac{\rho \bar{u_i}^2}{2}} = 4\left[1 - \frac{1}{Re_w}\right] \tag{2–58}$$

$$Re_w = \frac{a\int_0^L v dz}{L\nu} \tag{2–59}$$

where in this case Re_w is a wall flow parameter that allows for a non-constant radial wall velocity. This solution was produced by dividing the tube up into segments and assuming that the parabolic axial velocity profile is reduced in magnitude by a constant for each section due to suction.

By assuming that the wall velocity v_w was small and the tube length L was large so that a similarity solution was applicable, Oxarango et al. (2004) applied an averaging method to the Navier-Stokes equations and retained the inertial terms $u(\partial u/\partial x)$ and $v(\partial u/\partial r)$. The equations were then solved using a finite difference scheme for a dead-ended tube. The model showed that the axial pressure drop in the tube was smaller when these terms were included, although not greatly. The inclusion of a pressure-dependent v_w was also discussed, as well as applying the model to various multi-channel filtration systems. The model was shown to have good agreement with CFD results.

Clearly, there is a wide variety of possible solution methods for determining the flow field within a porous tube, depending on the flow regime and the model complexity desired. Of critical importance is the determination of whether the fully developed assumption is valid for the particular tube being examined, as can be seen by the volume of literature dealing with the topic. The range of Re_w anticipated also has a significant impact on the solution set available. While the more complex numerical solutions are likely to be quite accurate, very little experimental data has been collected to assess when simpler similarity solutions cease to be valid and numerical methods must be used to achieve accurate predictions. Furthermore, of the experimental data collected, the majority of it has been for large, sintered metal pipes, rather than small polymer membranes. Because of these trends, a practical engineering method for analyzing and selecting a given membrane for suitability in a particular application is a nebulous proposition at best. This work addresses the lack of literature, both in terms

of experimental data for polymer membranes as well as providing a practical method for satisfactorily predicting the behavior of membranes for the flow rates specified in Chapter 1.

2.2 Porous membrane modeling

While it is the focus of this work to study the flow inside of a tube with membrane walls and not flow through the actual membrane wall itself, a brief look at the state of the art in membrane modeling is warranted so as to shed some light on the wall boundary condition at $r = R$. In comparison to the literature covering flow through a porous tube, the literature for membrane modeling is much more unified. A significant work on modern membrane modeling is that of Mason et al. (1967) and more thoroughly again in Mason and Malinauskas (1983), upon which much of the subsequent membrane literature is based. In it, the "dusty-gas model" is introduced, which provides the foundation for most future theoretical work. The dusty gas model (DGM) is a method of describing flow through membranes by modeling the solid membrane as large, unmoving "dust" particles and using kinetic theory to determine how gases interact and pass by them. According to the model, there are three primary modes of transport through the porous medium:

- Diffusive transport, due to concentration gradients and limited by the membrane's diffusivity.
- Viscous transport, due to pressure gradients and limited by pore geometry and fluid viscosity (as discussed in Section 1.2.2).
- Knudsen diffusion, becoming significant when the mean free path of the fluid particles is on the same order as the pore size.

Note that each of these modes of transport can be described individually using prior models (Fick's law for diffusion, the Hagen-Poiseuille equation for viscous transport, etc —these models are described in detail by Mulder (1996)). However, the DGM, starting with kinetic theory, can be used to derive these relationships,

adding to their legitimacy. For instance, in the case of pressure-driven viscous transport through a membrane, where diffusive and Knudsen transport are insignificant, the transport equation is:

$$J'' = B_0 \frac{n\Delta P}{\mu t} \tag{2–60}$$

where J'' is the molar flux and B_0 is a lumped geometric term. Rewriting this in terms of a volumetric flux results in Equation 1–19. Hence, Mason and Malinauskas show that the simplified model presented in Section 1.2.2 is confirmed by using the kinetic theory and the DGM.

Despite the significant body of work on the subject of membrane modeling (Lawson and Lloyd (1997) provides a good review), it is clear that the most accurate and practical approach to modeling a given membrane is to characterize a sample membrane in an experiment that matches that of the intended application, as described by Mason and Malinauskas (1983). This is especially true in the case of porous polymer membranes, whose microscopic geometry is complex, random, and difficult to measure. A method to determine the pore size distribution of a membrane sample was detailed by McGuire et al. (1995), which involved measuring the flow rate of a pressurized liquid on one side of the membrane and calculating the pore size necessary for that pressure to overcome the capillary pressure of the pores. However, this measurement is of limited usefulness in terms of predicting membrane behavior in specific applications, as there is no direct link between pore size distribution and any macroscopic flow parameters such as k_D.

In conclusion, the state of the art in modeling pressure-driven membrane flow calls for first characterizing membrane samples to determine the permeability coefficient k_D (for volumetric flux) or B_0 (for molar flux) and use either Equation

1–19 or 2–60 to find the flux through the membrane. This can then be used as a boundary condition for analysis of the flow field in the membrane tube.

CHAPTER 3
MODELING

3.1 Assumptions

As shown in Table 1-1, the range of flow rates and tube diameters used in this study limits the inlet Reynolds numbers $Re_D = \overline{u}_i D/\nu$ to values in the laminar range. For this analysis, the following assumptions are made:

1. The inlet flow is assumed to be steady-state, fully-developed flow with a Hagen-Poiseuille parabolic velocity profile established in an upstream non-porous circular tube, which smoothly transitions into the porous section of the same diameter.

2. The porous tube length L is much greater than the inner diameter D, so that the flow is fully-developed (as explained on page 7) for a significant portion of the porous tube length (not to be confused with Assumption 1, which assumes a Hagen-Poiseuille profile at the inlet to the porous section).

3. The pressure outside the membrane p_{ext} is constant.

4. At the tube wall, the no-slip condition applies (as shown by Belfort and Nagata (1985)) for the axial velocity ($u_w = u(r = R, z) = 0$) and the radial velocity $v_w = v(r = R, z)$ is governed by the pressure drop across the membrane wall, $\Delta p_{mem} = p(z) - p_{ext}$.

5. Diffusion effects in the membrane are negligible, which is shown in an analysis given in Appendix A.

6. Knudsen diffusion effects in the membrane are negligible, as Knudsen diffusion is only significant when the mean free path of the gas approaches the pore diameter. Since at atmospheric pressure, the mean free path of carbon dioxide is on the order of nanometers and the pore size of the membrane is on the order on microns, this assumption is valid.

As discussed in Section 1.1, two primary flow properties are sought in this analysis: (1) the volumetric flow rate through the membrane wall $\dot{Q}_{mem}$ and (2) the axial pressure drop through the tube $\Delta p_z = p(0) - p(L)$.

3.2 Membrane flow rate

The rate of flow through the membrane wall is governed by the pressure difference across the membrane via Darcy's Law in Equation 1–19. Noting that the wall volumetric flux is equivalent to the average wall velocity, Equation 1–19 becomes:

$$\overline{v}_w = \frac{k_D}{\mu t}(p_i - p_{ext}) = \frac{k_D}{\mu t}\Delta p_{mem} \tag{3–1}$$

Non-dimensionalizing this in terms of λ_D:

$$-\frac{\overline{v}_w d}{\nu} = -\frac{k_D}{\mu t}\Delta p_{mem}\left(\frac{d}{\nu}\right) \tag{3–2}$$

$$\lambda_D = -\frac{k_D \rho d}{\mu^2 t}\left(\Delta p_{mem}\right) \tag{3–3}$$

$$\lambda_D = K \Delta p_{mem} \tag{3–4}$$

where $\lambda_D = -\overline{v}_w d/\nu$ and $K = -(k_D \rho d)/(\mu^2 t)$ is the dimensionless membrane permeability, somewhat similar to A in Equation 2–53 presented by Hornbeck et al. (1963). Using this relationship, the wall velocity for a given membrane and conditions can be calculated, and hence the flow rate through the membrane.

3.3 Axial pressure drop

As shown in Equation 1–6, the axial pressure drop is influenced by viscous forces brought on by the wall shear stress and momentum transport effects induced by the slowing of the flow as mass flow through the tube is reduced by wall extraction. Examining the tube control volume in Figure 3-1, the integrated form of the continuity equation results in:

$$\overline{u}_{out} A_{out} = \overline{u}_i A_{in} - \overline{v}_w A_s \tag{3–5}$$

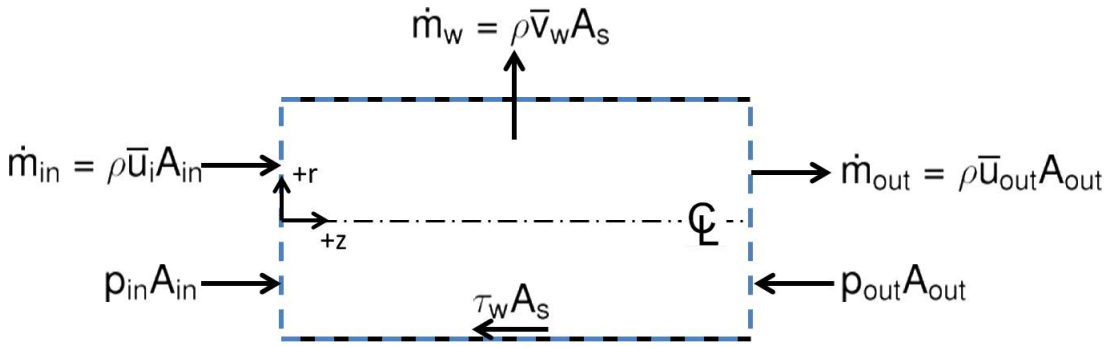

Figure 3-1. Momentum inputs and outputs for tube control volume

Assuming the flow is steady-state, incompressible, and fully-developed (Assumption 1), the integrated momentum equation in the z direction is:

$$\begin{aligned} 0 &= \dot{m}_{in} u_i - \dot{m}_{out} u_{out} + p_{in} A_{in} - p_{out} A_{out} - \tau_w A_s \\ 0 &= \rho \overline{u}_i^2 A_{in} - \rho \overline{u}_{out}^2 A_{out} + p_{in} A_{in} - p_{out} A_{out} - \tau_w A_s \end{aligned} \tag{3–6}$$

where τ_w is the wall shear stress, A_s is the surface area, and A_{in} and A_{out} are cross-sectional areas of the tube. Combining Equations 3–5 and 3–6 and solving for the pressure drop:

$$0 = \overline{u}_i^2 A_{in} - \left(\frac{\overline{u}_i A_{in} - \overline{v}_w A_s}{A_{out}} \right)^2 A_{out} + \frac{p_{in} A_{in}}{\rho} - \frac{p_{out} A_{out}}{\rho} - \frac{\tau_w A_s}{\rho} \tag{3–7}$$

Expanding the squared term:

$$0 = \overline{u}_i^2 A_{in} - \overline{u}_i^2 \frac{A_{in}^2}{A_{out}} + \frac{2 \overline{u}_i \overline{v}_w A_{in} A_s}{A_{out}} - \overline{v}_w^2 \frac{A_s^2}{A_{out}} + \frac{p_{in} A_{in}}{\rho} - \frac{p_{out} A_{out}}{\rho} - \frac{\tau_w A_s}{\rho} \tag{3–8}$$

Rearranging and dividing by $\rho \overline{u}_i^2 / 2$:

$$\frac{p_{in} A_{in} - p_{out} A_{out}}{\frac{1}{2} \rho \overline{u}_i^2} = 2 A_{in} \left(\frac{A_{in}}{A_{out}} - 1 \right) - \frac{4 \overline{v}_w A_{in} A_s}{\overline{u}_i A_{out}} + \frac{2 \overline{v}_w^2}{\overline{u}_i^2} \frac{A_s^2}{A_{out}} + \frac{\tau_w}{\frac{1}{2} \rho \overline{u}_i^2} A_s \tag{3–9}$$

Defining the skin friction coefficient as $c_f \equiv \tau_w / (\frac{1}{2} \rho \overline{u}_i^2)$ simplifies this to:

$$\frac{p_{in} A_{in} - p_{out} A_{out}}{\frac{1}{2} \rho \overline{u}_i^2} = 2 A_{in} \left(\frac{A_{in}}{A_{out}} - 1 \right) - \frac{4 \overline{v}_w A_{in} A_s}{\overline{u}_i A_{out}} + \frac{2 \overline{v}_w^2}{\overline{u}_i^2} \frac{A_s^2}{A_{out}} + c_f A_s \tag{3–10}$$

If the tube has a constant cross-sectional area, Equation 3–10 can be simplified by letting $A_{in} = A_{out} = A_c$:

$$\Delta\widehat{p}_z = \frac{\Delta p_z}{\frac{1}{2}\rho\overline{u}_i^2} = \frac{2\overline{v}_w^2}{\overline{u}_i^2}\left(\frac{A_s}{A_c}\right)^2 - \frac{4\overline{v}_w}{\overline{u}_i}\frac{A_s}{A_c} + c_f\frac{A_s}{A_c} \tag{3–11}$$

where $\Delta p_z = p_{in} - p_{out}$.

Equation 3–11 provides a means to calculate the dimensionless axial pressure drop, $\Delta\widehat{p}_z$, with knowledge of average entrance velocity $\overline{u}_i$, the average velocity through the wall, $\overline{v}_w$, the tube geometry, and the skin friction coefficient c_f. At this point, the only remaining unknown is c_f. An analysis performed by Kinney (1968) isolated the effect of c_f for a porous tube, which is reproduced in Appendix B. An empirical correlation for $c_f Re$ as a function of λ_D has been determined by Raithby (1971), which was shown in Equation 2–24 and again here:

$$c_f Re_D = \left(0.0481 + \frac{0.0494}{(\lambda_D + 4.70)^{0.800}}\right)^{-1} \tag{3–12}$$

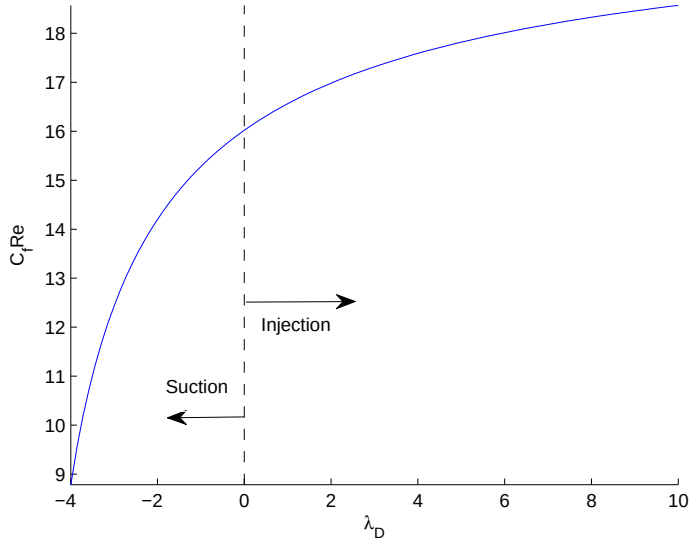

Figure 3-2. Relationship between skin friction coefficient and wall flow parameter, as defined by Raithby (1971)

This relationship is mathematically valid for $\lambda_D > -4.7$, and is shown in Figure 3-2. Note that when $\lambda_D = 0$ (meaning no flow through the wall), $c_f Re = 16$, which corresponds to the established Darcy friction factor relationship for laminar flow through a non-porous tube:

$$f = 4c_f = \frac{64}{Re_D} \tag{3–13}$$

Inserting this value of c_f and $v_w = 0$ into Equation 3–11 then yields the Hagen-Poiseuille relationship for laminar flow with a non-porous tube:

$$\Delta p_z = \frac{8\mu L\dot{Q}}{\pi R^4} \tag{3–14}$$

Using the relationship in Equation 3–12, c_f can be solved by calculating $\overline{v}_w$ using Equation 3–4. The axial pressure drop can then be calculated using Equation 3–11.

CHAPTER 4
EXPERIMENT

As the objective of this work is to specify a process for selecting a membrane that produces flow characteristics desirable for a specific application, two experiments are detailed here:

1. A membrane characterization experiment, which is an experiment meant to measure the permeability coefficient, k_D, of a membrane sample by dead-ending the membrane tube and measuring the internal pressure and flow rate through the membrane walls, as described in Section 4.1 below.

2. A validation experiment, where the membrane is placed in a flow-through setup as it would be if employed in an engineering application. In this case, gas flows through the membrane and is free to exit through the tube's end, as described in Section 4.2. The flow rate through the membrane wall and the axial pressure drop are measured and the proposed model in Chapter 3 is assessed for validity.

4.1 Membrane characterization

The experiment to characterize the k_D of the membrane tube is similar to the experiments of Quaile and Levy (1972). Characterization of the membrane tube was accomplished by dead-ending the tube and measuring the pressure just prior to the tube entrance at $z = 0$ and at the tube end at $z = L$. The volumetric flow rate into the sample was measured using a rotameter. The experimental setup is shown in Figure 4-1. The sample tube length was selected in order to achieve a relatively constant static pressure throughout the tube and therefore a constant pressure drop across the membrane for all points in the tube; the purpose of this arrangement is to induce a constant v_w throughout the sample. Referring to the numerical solution of Galowin et al. (1973), the pressure is relatively constant for all points when $Re_w \leq 1$, however, depending on the desired flow rate, this may

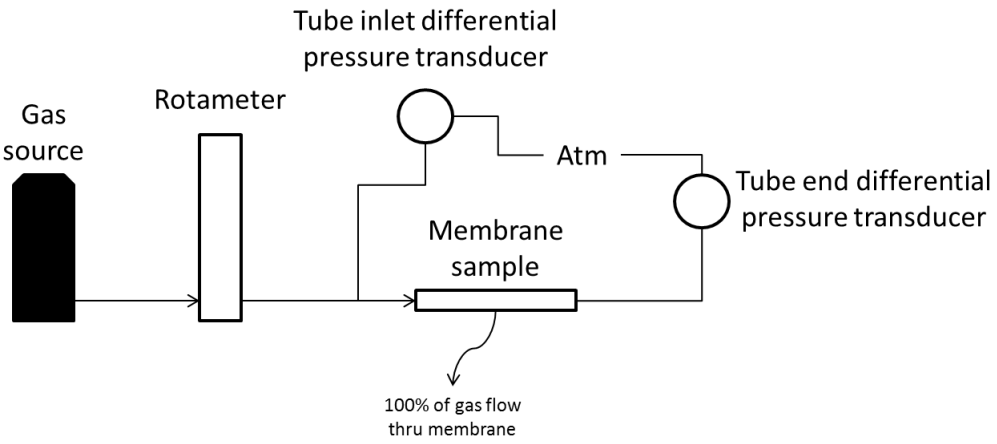

Figure 4-1. Schematic of membrane characterization test

result in a prohibitively long tube length and even then, Re_w may not be constant for the entire tube length. The requirements for measuring an accurate value of k_D is examined in Chapter 5. It should also be noted that measurement of the inlet and exit pressures is redundant if the pressure is known to be relatively constant through the length of the tube; here it is used as a method to check the validity of the $Re_w \leq 1$ condition.

In this work, carbon dioxide was used as the gas at flow rates between 100 and 500 sccm. The exterior pressure p_{ext} was atmospheric, and all pressure measurements were differential and referenced to p_{ext}. The permeability coefficient k_D was determined by measuring the flow rate $\dot{Q}$ and the pressure across the membrane wall Δp_{mem} and employing Equation 1–19. For a particular gas viscosity and membrane thickness, Equation 1–19 predicts that $\dot{Q}$ is linear with Δp_{mem} so that the resulting slope of a $\dot{Q}$ versus $\Delta p_{mem}/(\mu t)$ graph will be k_D.

It is important to characterize the membrane's behavior at the absolute pressure and temperature of the application, as the polymer membrane may undergo dimensional changes due to stretching or compression brought on by extreme conditions due to the polymer membrane's structural limitations. This effect was studied by Lawson et al. (1995), who also provided a model for

predicting the effect of membrane compaction. Finally, because the manufacturing process may introduce a degree of variability in the pore geometry, multiple samples should be characterized to understand the range of k_D for a particular membrane.

4.2 Pressure drop and through-membrane flow

After k_D is determined for a membrane, the experimental setup was altered by removing the blockage at the end of the tube and permitting flow to pass freely through the far end of the tube at $z = L$. This change and the additional instrumentation included in this test is shown in Figure 4-2. The inflow of gas $\dot{Q}_{in}$ is set by a digital flow controller and the tube outflow $\dot{Q}_{out}$ is measured by a rotameter. The axial pressure drop Δp_z and pressure drop across the membrane Δp_{mem} are measured with pressure transducers as shown. The axial pressure drop transducer has a range of 0 to 0.75 inH_2O and the membrane pressure drop transducer's range is 0 to 10 inH_2O.

The exterior pressure p_{ext} is atmospheric, so Δp_{mem} is varied using the built-in rotameter valve to increase the back pressure inside the tube. After passing through the rotameter, the remaining flow is dumped to atmosphere. As with the membrane characterization experiment, all flow-through experiments were performed at room temperature (21° C), and the gas used in all testing was carbon dioxide.

The closest comparison of this experiment in the published literature is that of Bundy and Weissberg (1970); however, in addition to the differences in membrane material (Bundy and Weissberg used a sintered metal pipe), that experiment also dealt strictly with injection through the membrane, rather than flow out of it. Furthermore, due to the structural constraints of the thin polymer membrane, the positioning of pressure taps throughout the length of the tube was not possible, leading to the entrance and exit pressure taps as shown in

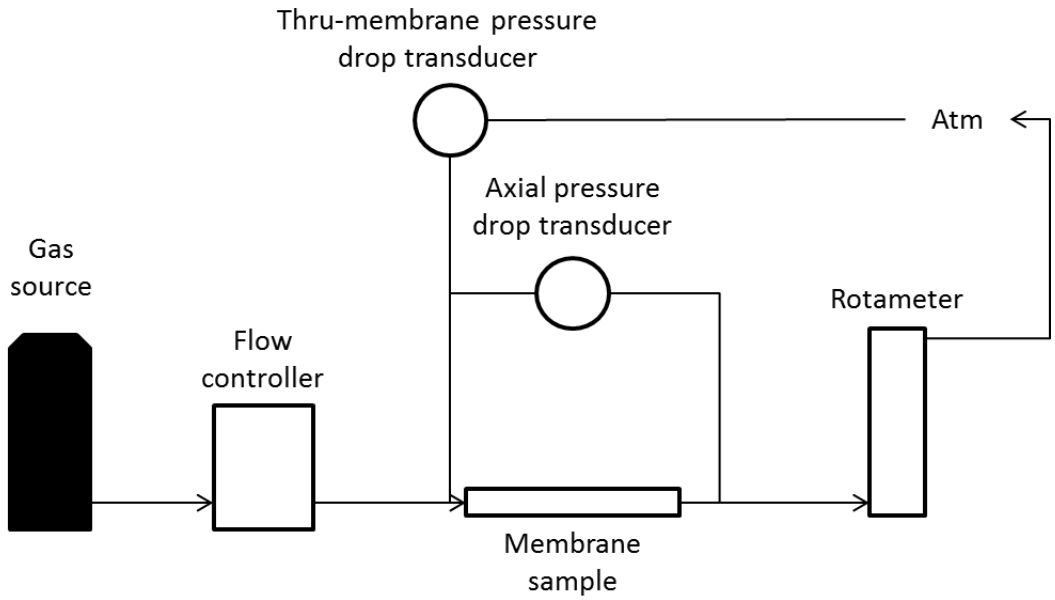

Figure 4-2. Schematic of validation experiment

Figure 4-2. In order to examine the z dependence of the pressure, various tube lengths were used. While Brady (1984) does state that the exit velocity profile can have an effect on the flow field upstream in the tube, this was determined to not be true for $Re_w < 2.3$, which is the flow regime of interest here, as shown in Table 4-1. Table 4-1 shows the maximum Reynolds number Re_D for each diameter of porous tube, which corresponds to the maximum inlet flow rate of 450 sccm. The maximum possible Re_w is calculated for a tube length of 10 cm, which corresponds to the extreme case of 100% of the flow exiting through the tube walls. Naturally, this value will decrease as L increases and as the percentage of flow that does not escape through the tube wall increases.

	TB0302	TB1008
Inner diameter	2 mm	8 mm
Maximum flow rate	500 sccm	500 sccm
Maximum Re_D	644	161
Maximum Re_w for L =10 cm	1.6	1.6

Table 4-1. Maximum values for various flow parameters

CHAPTER 5
RESULTS AND DISCUSSION

5.1 Membrane characterization

The characterization data for various samples of TB0302 and TB1008 (see Table 1-1 for tube definitions) are shown in Figures 5-1 and 5-2. As stated in Section 4.1, a goal of the characterization was for the axial pressure drop Δp_z to remain low compared to Δp_{mem} so as to provide a constant Δp_{mem} throughout the porous tube. For all data collected, Δp_z was never more than 4.5% of Δp_{mem}, which satisfies this condition. Interestingly, this was true even for Re_w as high as 3.4, which conflicts with the numerical solution of Galowin et al. (1973) discussed in the previous chapter. As expected from Equation 1–19, v_w is linear with respect to $\Delta P_{mem}/(\mu t)$, with a slope of k_D. In fact, these two membrane types have

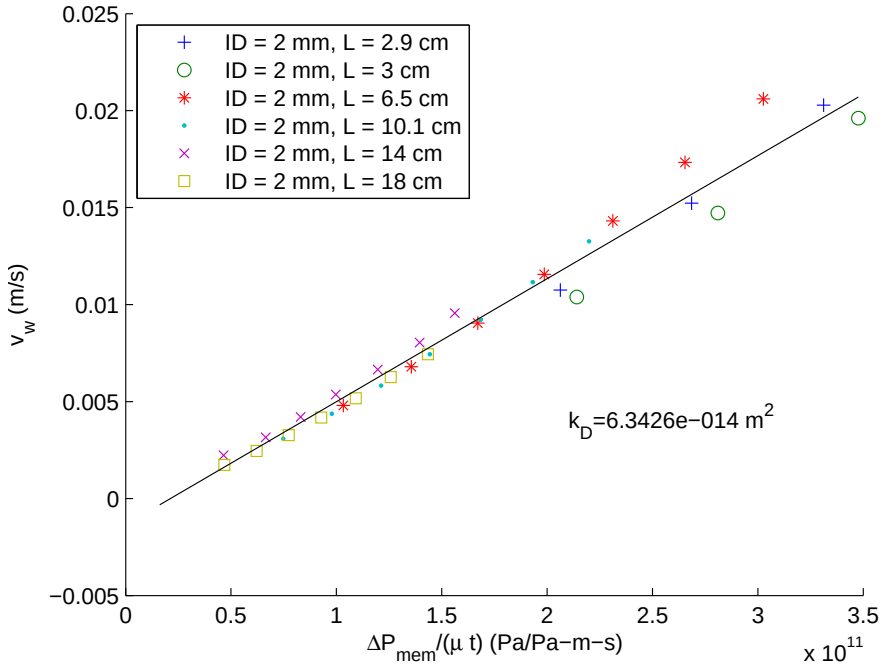

Figure 5-1. Membrane characterization plot for TB0302

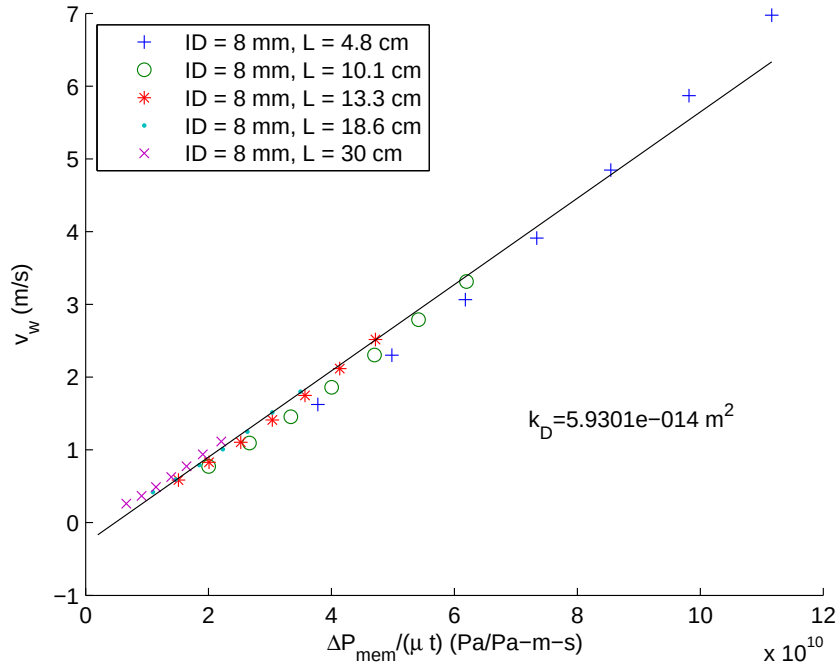

Figure 5-2. Membrane characterization plot for TB1008

the same k_D value, as can be seen in Figure 5-3. This is not surprising, as the membranes are merely different sized versions of the same membrane material produced by a single manufacturer. However, it is interesting to note that the manufacturer-specified porosities, ϵ, from Table 1-1 for TB0302 and TB1008 are 0.6 and 0.8 respectively. Comparing Equations 1–18 and 1–19, it would be expected that k_D would have a dependence on ϵ, however, either that is not the case here, the specified porosity is incorrect, or the tortuosity and pore size distribution change enough to negate the change in porosity. This discrepancy serves to reinforce the necessity of characterizing membrane samples prior to engaging in any predictive calculations.

Since the slopes shown in Figures 5-1 and 5-2 are essentially the same, the data for both TB0302 and TB1008 can be plotted together to determine an “overall” value of k_D, as is shown in Figure 5-3. Upon closer examination, it can be seen that samples with shorter lengths L have a slightly lower slope than the overall trend shown in Figure 5-3. In addition, the y-intercepts for

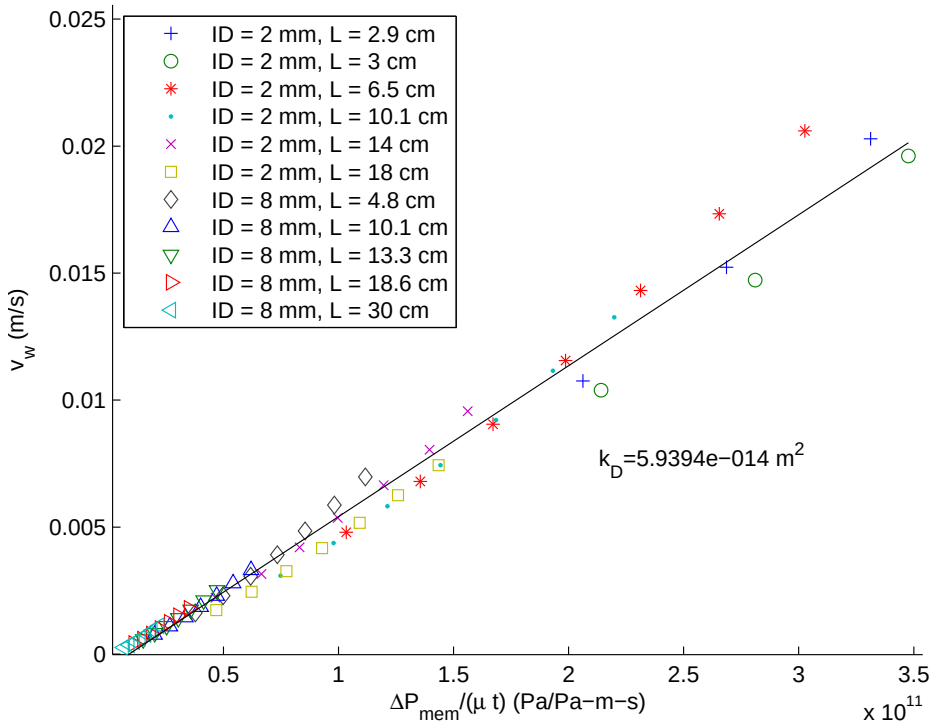

Figure 5-3. Membrane characterization plot for all TB0302 and TB1008 data

these shorter tube lengths are more negative, with progressively longer tube lengths corresponding to intercepts that approach zero. (Contributions from these shorter tube lengths to the overall best fit line can be seen in Figures 5-1 through 5-3, where the best fit line does not pass through zero.) This trend is shown in clearer detail in Figure 5-4, where the percent difference between the k_D for each particular sample and the overall k_D is compared as a function of the dimensionless length $\widehat{L} = L/(dRe_D)$. As can be seen, as dimensionless length increases, the difference approaches zero, meaning that the sample k_D approaches that of the overall k_D. The point at which the sample k_D matches the overall k_D within 5% appears to be at approximately $\widehat{L} = 0.23$ for TB0302 and $\widehat{L} = 0.13$ for TB1008. The discrepancy between these two values could be caused by inconsistencies in the tube geometry, either in the form of variations in inner diameter or wall thickness, or possibly even changes in these features

due to stretching of the membrane material from pressurization during testing. However, given these data, a conservative conclusion to make is that for $\widehat{L} \geq 0.3$, k_D is a constant value for the tube, meaning two things:

1. The fully-developed assumption is appropriate for these tube lengths. Note that this does not mean that $\widehat{L} \geq 0.3$ is a relationship for hydrodynamic entrance length — rather, that for these lengths, the tube is satisfactorily long such that fully developed flow (as explained on page 7) exists in enough of the tube to make modeling using the fully developed assumption valid.

2. That using an average wall velocity v_w is valid at these tube lengths. The assumption that v_w is constant for every point along the tube length is not necessarily true, but there exists an average value of v_w that is representative of the entire tube that can be used in calculations.

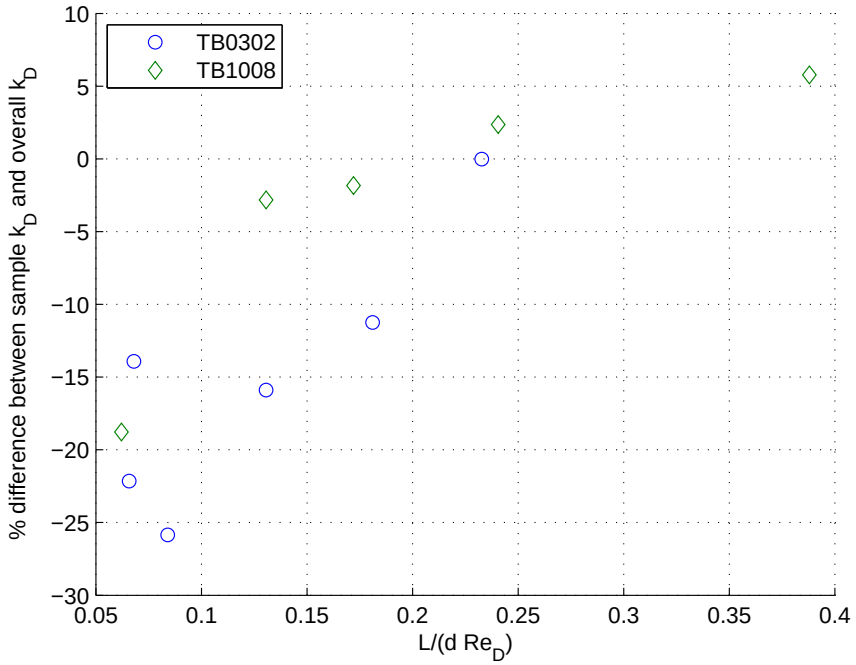

Figure 5-4. Percent difference between permeability coefficient k_D for a specific sample and the overall permeability coefficient shown in Figure 5-3

5.2 Evaluation of flow-through model

5.2.1 Membrane flow rate

Data collected for through-membrane flow rate for both TB0302 and TB1008 are shown in Figures 5-5 and 5-6. The through-membrane flow rate is expressed

in terms of λ_D versus Δp_{mem}, so that the linear relationship predicted in Equation 3–4 can be seen. Note that, since λ_D is negative for outflow, increasing through-membrane pressures result in higher through-membrane flow and therefore, increasingly negative values of λ_D. From Equation 3–4, one would expect that the slope of the best fit line to each of these plots would be equal to $K = -(k_D \rho d)/(\mu^2 t)$, the modified permeability coefficient. As seen in Table 5-1, the data for TB1008 fits this quite well, however there is a significant difference between the calculated K value and the line fit of the data for TB0302.

	TB0302	TB1008
K	-0.0020 Pa^{-1}	-0.0039 Pa^{-1}
Best fit line slope	-0.0027 Pa^{-1}	-0.0042 Pa^{-1}
% difference	25.9%	7.1%

Table 5-1. Comparison of calculated K with slope of the best fit line

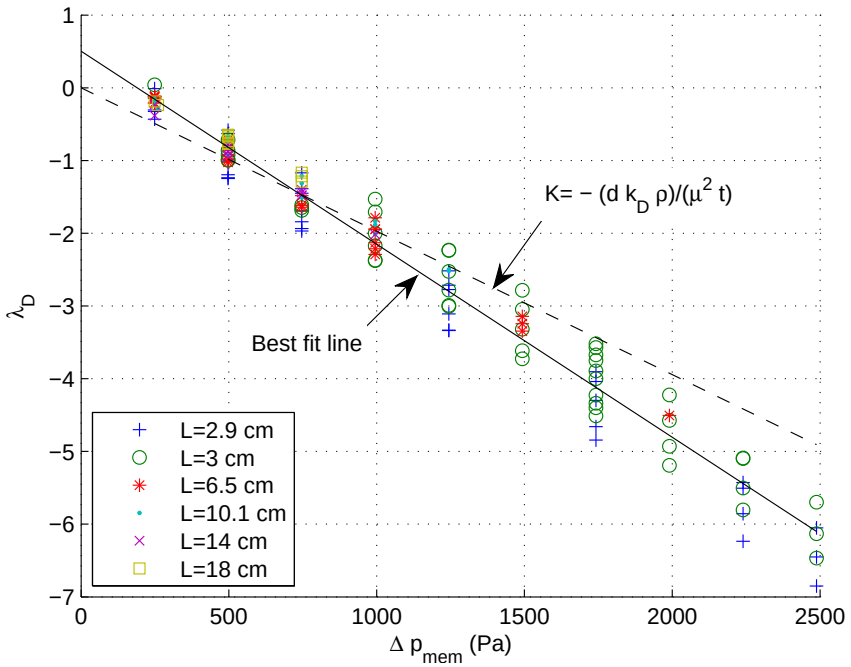

Figure 5-5. Wall flow parameter λ_D versus through-membrane pressure drop for TB0302

A similar treatment to the one used in the previous section can be applied here to examine the entrance length. The percent difference between the slope of

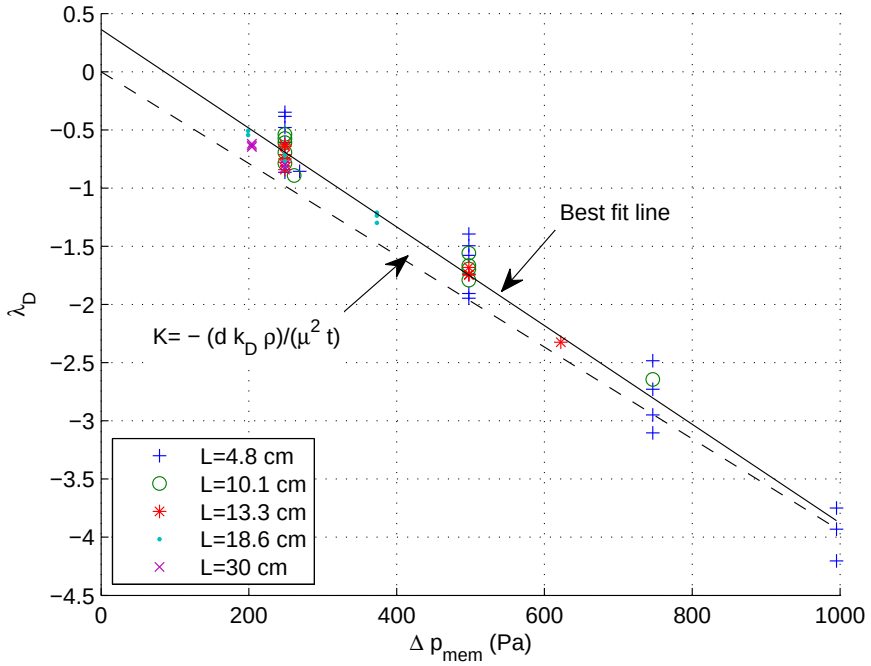

Figure 5-6. Wall flow parameter λ_D versus through-membrane pressure drop for TB1008

the data in Figures 5-5 and 5-6 to that of the modified permeability coefficient K and plotting as a function of dimensionless length $\widehat{L}$ results in Figure 5-7. Similar to the trend in Figure 5-4, as $\widehat{L}$ increases, the slope of λ_D vs Δp_{mem} approaches K, again lending itself to the conclusion that once the dimensionless length becomes sufficiently large, enough of the flow in the tube is fully developed for the fully developed assumption to provide an accurate representation of entire tube flow. As can be seen in Figure 5-7, the percent difference between the slope of the data and K becomes less than 5% when $\widehat{L} = 0.14$ for TB1008 and $\widehat{L} = 0.21$ for TB0302. Conservatively, the minimum value for the fully-developed flow assumption to be valid in open-ended tube flow could again be placed at $\widehat{L} = 0.3$. (Note that this value of $\widehat{L}$ agrees with the results of Section 5.1. This value will be revisited and confirmed again in the axial pressure results in Section 5.2.2.) This value is an order of magnitude larger than to the results of Hornbeck et al. (1963), whose numerical solution predicted that the entrance length for a

porous tube with a parabolic inlet velocity profile was $\widehat{L} = 0.0348$ for $\lambda_D = -2$, which compares closely to the entry length for laminar flow in a non-porous tube, $\widehat{L} = 0.0288$ (Eckert and Drake, 1959). However, it must be stressed that the value $\widehat{L} = 0.0288$ for a non-porous tube and $\widehat{L} = 0.0348$ for a porous tube ($\lambda_D = -2$) are the exact entry lengths, whereas the value of $\widehat{L} = 0.3$ inferred from the data is the value necessary for a fully-developed model to predict the data within 5%. This implies that the porous tube must be at least 10 times the length of the entry region for a fully developed model to accurately predict the data. Therefore, when $\widehat{L} \geq 0.3$, Equation 3–4 can be used to predict v_w and subsequently $\dot{Q}_{mem}$ within 5% using the modified permeability coefficient K.

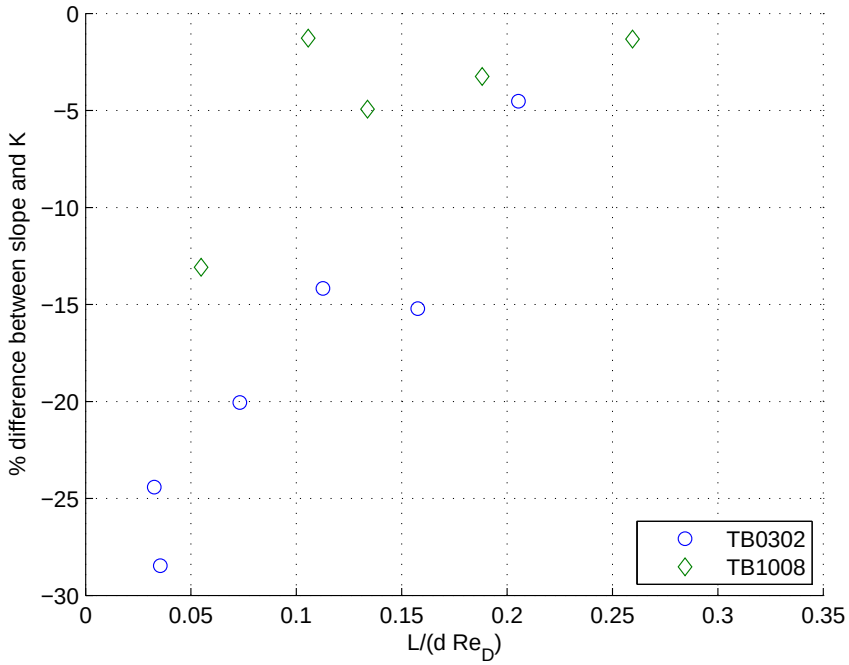

Figure 5-7. Percent difference between modified permeability coefficient K and best fit slope of the wall flow parameter λ_D as a function of dimensionless tube length $\widehat{L}$

5.2.2 Axial pressure drop

The results for axial pressure drop for the larger diameter tubing TB1008 were too small to be accurately measured (on the order of 10^{-3}), and thus, only the data for TB0302 will be examined here. The results for the axial pressure

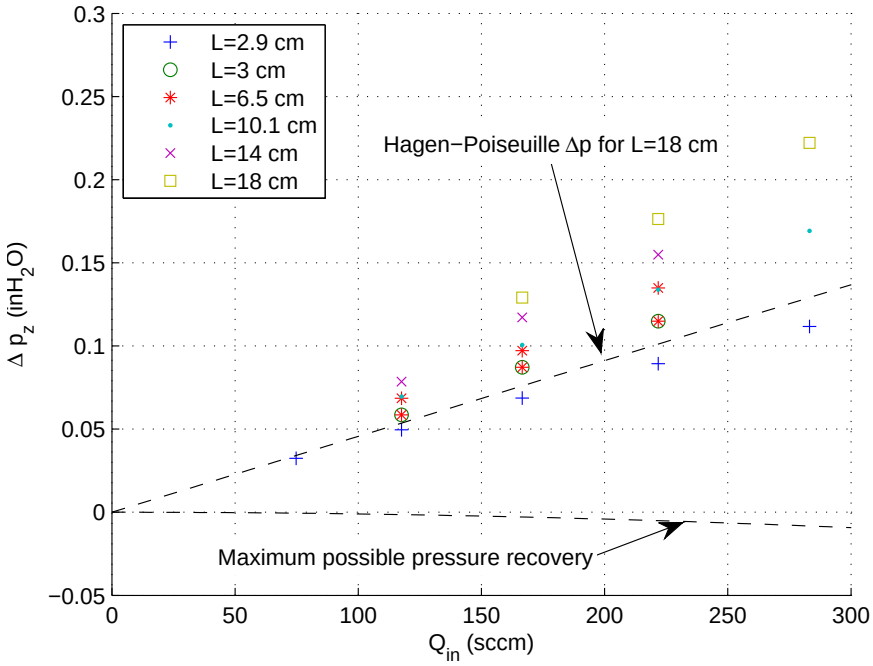

Figure 5-8. Measured axial pressure drop as a function of inlet flow rate for Δp_{mem} =1 inH$_2$O for TB0302

drop Δp_z for Δp_{mem} =1 inH$_2$O are shown in Figure 5-8. As can be seen, for a given Δp_{mem}, higher inlet flows result in higher axial pressure drops. For reference, the pressure drop predicted by the Hagen-Poiseuille equation for the same diameter and maximum length of non-porous tube is plotted, as well as the maximum potential static pressure that could be recovered from slowing the flow to a complete stop without any losses, corresponding to $\Delta p = -(\rho \overline{u}_i)/2$. Note that the measured pressure drop for the porous tubes is significantly higher than what is predicted for the non-porous tube, indicating that the outflow at the tube wall is inducing losses in the flow in addition to that of the wall friction. As can be seen by the “Maximum possible pressure recovery” line, at such low inlet flow rates, the amount of dynamic pressure that is available to be recovered into static pressure as the flow slows is much smaller than the pressure loss created by the wall friction. This leads to the conclusion that, for these flow rates, the relative

strength of the wall friction term, $c_f Re_D$, in Equation 2–22, is much higher than that of the momentum term, $4\beta\lambda_D$.

The data can be put into a more readable form by plotting dimensionless axial pressure drop Γ (as defined in Equation 2–20) as a function of tube length for several selected Δp_{mem}, as shown in Figure 5-9. As can be seen, Γ is much

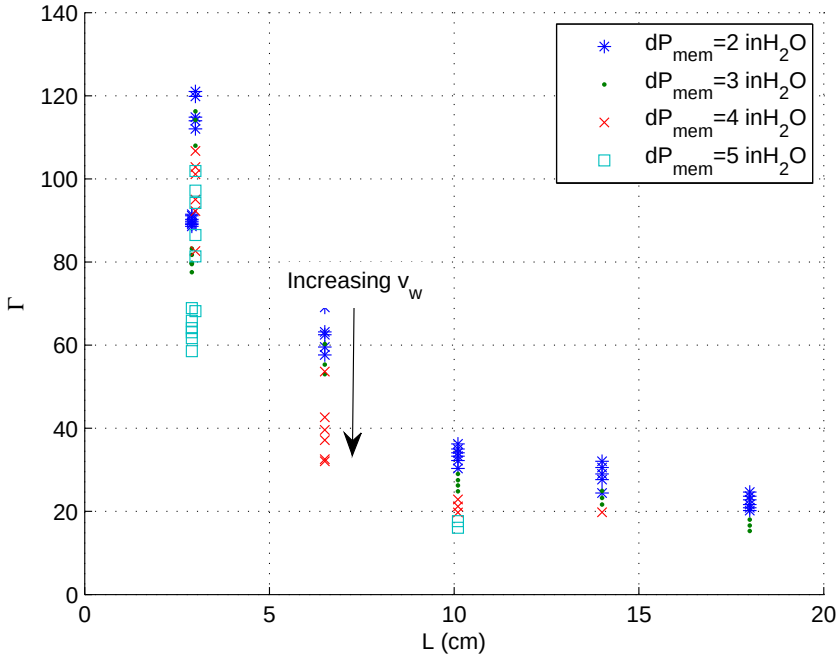

Figure 5-9. Dimensionless axial pressure drop Γ versus tube length L for selected through-membrane pressures for TB0302

higher for shorter lengths of tube and quickly settles to a low value as length increases. (Note that the reason that Γ decreases with increasing length is due to the fact that Γ is normalized by the tube length, L. The actual axial pressure drop, Δp_z, increases with tube length, as illustrated in Figure 5-8.) Furthermore, increasing Δp_{mem} and therefore v_w has the effect of further decreasing Γ. This makes intuitive sense: the higher v_w, the more fluid is extracted from the tube, slowing the flow and recovering more velocity head into static pressure. Figure 5-9 indicates, however, that this is a secondary effect, which is to be expected from the relative weakness of the pressure recovery effect, which was shown

in Figure 5-8. Additionally, recalling Figure 3-2 and the relationship for $c_f Re$, increasing values of suction λ_D result in lower values of $c_f Re$, meaning that, using the relationship of Kinney (1968), the skin friction will also be lower from increased outflow, further lowering the axial pressure drop.

Employing the method in Section 3.3 and Equation 3–11 to calculate the axial pressure drop Δp_z results in Figure 5-10, which shows the percent difference between the calculated and recorded value of $\Delta\widehat{p}_z = \Delta p_z/(\rho\overline{u}_i^2/2)$ as a function of $\widehat{L}$. As can be seen, the absolute value of the percent difference is

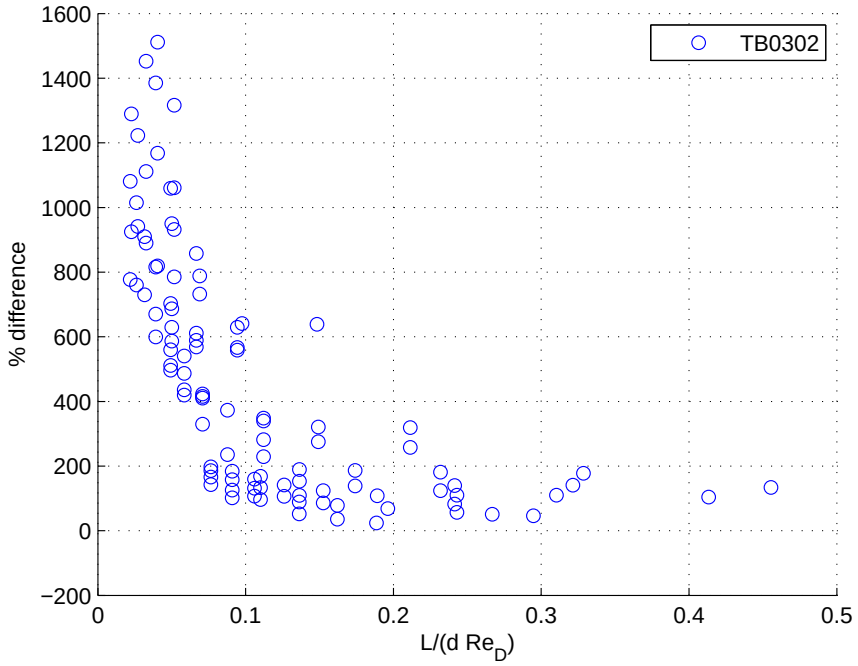

Figure 5-10. Percent difference between calculated and actual dimensionless axial pressure drop $\Delta\widehat{p}_z$ as a function of dimensionless tube length $\widehat{L}$ for TB0302

quite high, but undergoes a significant reduction as $\widehat{L}$ increases. Similar to the results of previous sections, the percent difference does reach its settling value by $\widehat{L} \approx 0.3$, however, the settling value is not zero as it was previously. Instead, the percent difference seems to settle on an offset value of approximately 100%; in other words, the actual pressure drop is twice that of what the calculations predict.

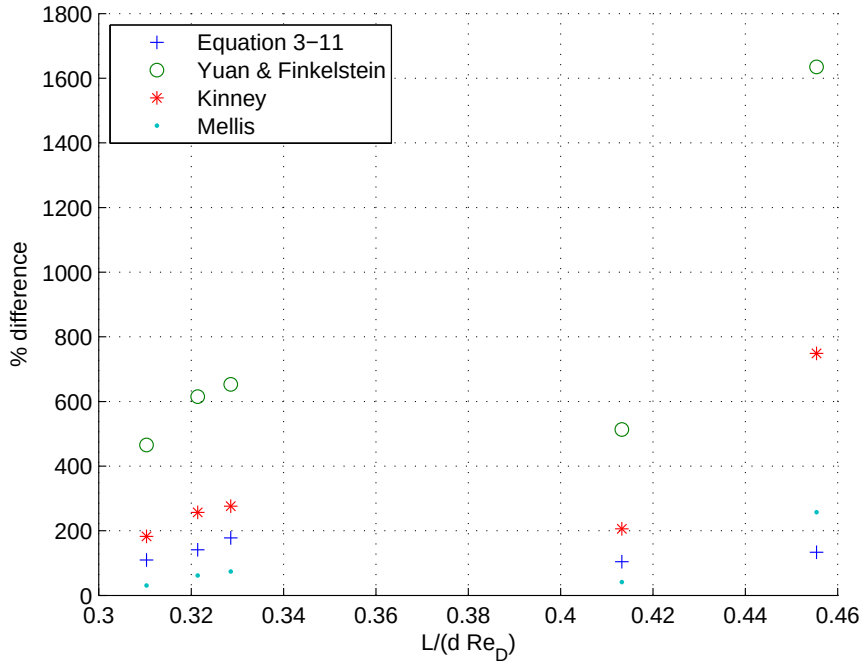

Figure 5-11. Percent difference between calculated and actual dimensionless axial pressure drop $\Delta\widehat{p}_z$ as calculated by this method and the methods of other authors for $\widehat{L} \geq 0.3$ for TB0302

A comparison of these results to the fully-developed methods of other authors for $\widehat{L} \geq 0.3$ is shown in Figure 5-11. All of these solutions similarly under-predict the experimental data (this conclusion is consistent with that of Mellis et al. (1993)). The most likely reason for this discrepancy is due to the fact that no developing entrance region was accounted for in each of these models, each of which assume that the flow was fully-developed and exclude any entrance effects. In non-porous tubes, the pressure drop in the developing region can be a significant contributor to the overall pressure drop, as shown by Eckert and Drake (1959). In the literature, solutions that solve for the developing region in porous tubes are exclusively numerical; therefore, if high resolution is desired in this region, a finite difference scheme, such as those by Hornbeck et al. (1963) or Brady (1984), or a similar numerical method must be implemented.

Since the model used to calculate the results in Figure 5-10 assumes that the flow is fully-developed, the existence of additional pressure drop in the

experimental data suggests that there is a significant pressure loss associated with the developing region. This hypothesis is empirically reinforced by the fact that the fully-developed solution predicts the pressure drop with a constant offset above $\widehat{L} \geq 0.3$. That is, once the tube length is longer than the length of the developing region, the axial pressure drop is the sum of the pressure loss from the developing region (a constant) and the pressure loss from the fully-developed region (which scales with tube length).

An estimate of the pressure loss induced by the developing region can therefore be made using the collected data. As it is done with non-porous tubes, assume that for tube lengths longer than the length of the developing region that the pressure drop in the porous tube is the sum of a pressure loss from the developing region and a pressure loss from the fully-developed region:

$$\Delta p_z = \Delta p_{z,developing} + \Delta p_{z,fully-developed} \tag{5–1}$$

The second term will scale with tube length and can be determined from Equation 3–11. The first term will be assumed to be a constant multiplied by the dynamic pressure (as it is for a non-porous tube in Eckert and Drake (1959)). Making these replacements in Equation 5–1 results in:

$$\Delta p_z = c_{ent}\frac{1}{2}\rho\overline{u}_i^2 + \Delta p_{z,fully-developed} \tag{5–2}$$

Where c_{ent} is a constant to be determined. (Note that $c_{ent} = 2.16$ for non-porous tubes (Eckert and Drake, 1959).) Expressing Equation 5–2 non-dimensionally,

$$\Delta\widehat{p}_z = c_{ent} + \left[\frac{2\overline{v}_w^2}{\overline{u}_i^2}\left(\frac{A_s}{A_c}\right)^2 - \frac{4\overline{v}_w}{\overline{u}_i}\frac{A_s}{A_c} + c_f\frac{A_s}{A_c}\right] \tag{5–3}$$

An appropriate value of c_{ent} can be determined by selecting a value such that the percent difference between the calculated and measured value of $\Delta\widehat{p}_z$ in Figure 5-10 settles to 0%. Using only the data for which $\widehat{L} \geq 0.3$ and a computer

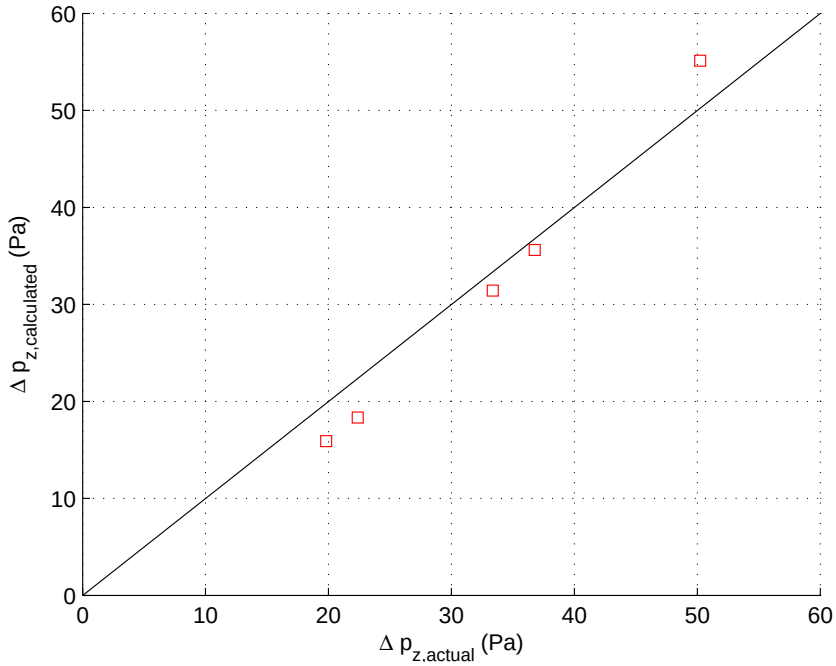

Figure 5-12. Results of Equation 5–3 compared to experimental data for $\widehat{L} \geq 0.3$ for TB0302, using a value of $c_{ent} = 24.6$

algorithm to find the value of c_{ent} that reduces the error between Equation 5–3 and the measured values, an average value of $c_{ent} = 24.6$ was determined. Modifying the results using Equation 5–3 and this value of c_{ent} for data points corresponding to $\widehat{L} \geq 0.3$ results in calculated values displayed in Figure 5-12. As can be seen, this modification results in the calculations much more closely matching the data for these dimensionless lengths. It should be noted that using Equation 5–3 for $\widehat{L} < 0.3$ is not appropriate, as these lengths are close to or within the developing region and the actual pressure drop will likely be less than that predicted by Equation 5–3.

CHAPTER 6
CONCLUSION

As stated in Section 1.1, the purpose of this work was to detail a characterization process for evaluating porous polymer membranes and to present a practical method for using this characterization data to predict membrane behavior in a specific application. Using the experimental setup in Section 4.1, a tube membrane's permeability coefficient k_D can be determined. The value of k_D can then be used to calculate the through-membrane flow rate $\dot{Q}_{mem}$ using Equation 3–4, provided that the tube length is sufficiently long such that fully developed flow exists in a significant portion of the tube length; the condition $\widehat{L} = L/(\rho Re_D) \geq 0.3$ has been shown to be sufficient for Equation 3–4 to be valid. For the range of flow rates tested, the through-wall and axial pressure drop were low enough that using a constant wall velocity, v_w, was sufficient to match the data, as shown in Figures 5-5 and 5-6. In terms of axial pressure drop, since the relationship in Equation 3–11, which assumed a fully-developed flow, under-predicted the data in a consistent manner when $\widehat{L} \geq 0.3$, it was assumed that a pressure drop accounting for the developing region must be included. Modifying Equation 3–11 to include this additional pressure drop resulted in Equation 5–3, and it was determined that using a pressure loss of $\Delta p_{z,developing} = 24.6\rho\overline{u}_i^2/2$ for the developing region resulted in a good fit between the data and the model. This is demonstrated in Figure 5-12.

An overview of the accuracy of the $\dot{Q}_{mem}$ calculations is given in Figure 6-1, where the calculated value and measured value of $\dot{Q}_{mem}$ and Δp_z are plotted. The points corresponding to the condition $\widehat{L} \geq 0.3$ are highlighted with a box around them. As can be seen the value of $\dot{Q}_{mem,calculated}$ generally fits the data

for the entire range of $\dot{Q}_{mem,measured}$. Furthermore, the points corresponding to the condition $\widehat{L} \geq 0.3$ do not tend to be more representative of reality than any of the other points. Therefore, for this range of flows and tube sizes, this method of determining $\dot{Q}_{mem}$ seems to be equally accurate regardless of the dimensionless length $\widehat{L}$.

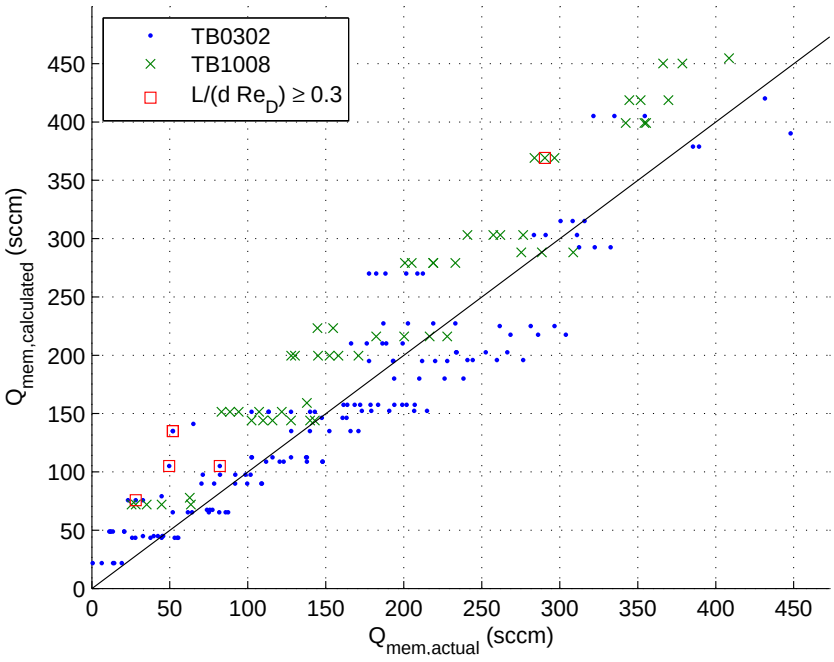

Figure 6-1. Comparison of the calculated value versus the measured value of the through-membrane flow rate $\dot{Q}_{mem}$ (Points corresponding to $\widehat{L} \geq 0.3$ are highlighted with a box around them)

The same cannot be said for the Δp_z calculation, as was shown in Figure 5-12 in the previous section. For $\widehat{L} < 0.3$, the predictions tended to overestimate Δp_z, which is likely because the flow had not yet become fully-developed and the full pressure drop from the developing region had not yet been realized. Therefore, it can be concluded that the relationship in Equation 5–3 is only valid when the dimensionless length is sufficiently large, that is, when $\widehat{L} \geq 0.3$. Note, however, the very small values for $\Delta p_{z,measured}$ in Figure 5-12; the highest value is 50 Pa (less than 10^{-3} atm). This means that if the design application requires

only an order of magnitude estimate for Δp_z, the Hagen-Poiseuille equation can be used to calculate an approximate answer, as was shown in Figure 5-8.

The method presented here is considerably simpler than most, if not all, of the solutions available in the literature. However, the ease of implementation does not degrade the quality of the match between the results and data, as seen when comparing this solution to that of other authors (see Figure 5-11). The method of membrane characterization, detailed in Section 4.1, has been shown to be effective in determining k_D and hence K, λ_D, v_w, and $\dot{Q}_{mem}$. It has also demonstrated the unreliability of the manufacturer's specifications, as the two tubes studied had different specified porosities, yet were determined to have identical permeability coefficients. Determination of Δp_z using Equation 5–3, while simplistic, offers a method of solution that is physically meaningful and quite accurate for $\widehat{L} \geq 0.3$, as seen in Figure 5-12. The comparison of this method against that of other fully-developed solutions in Figure 5-11 shows that no significant improvement is offered by other fully-developed solutions. In fact, judging from the literature, it can be speculated that if a higher accuracy is required, especially in the developing region, that a numerical solution such as that of Hornbeck et al. (1963) will be needed.

Future work in this area should focus on several areas:

- Developing an analytical solution for the length of the developing region, as well as the pressure loss associated with it.
- Investigation of a combined gas/liquid flow inside the tube to create a model useful for evaluating a porous polymer membrane tube as a gas-liquid separator, as described in Section 1.1.
- A materials study wherein the permeability coefficient k_D is correlated in some way to the membrane pore geometry, with the goal of making manufacturers' specifications more useful in predictive calculations.

Finally, given the relative lack of experimental data on this topic, especially when using a porous polymer membrane as the wall material, additional experimental

data is required to confirm model validity at other flow rates, pressures, and temperatures. Such information will prove valuable, as the applications for porous polymer membranes will likely continue to increase in the coming years.

APPENDIX A
VERIFICATION THAT DIFFUSION EFFECTS ARE NEGLIGIBLE

Diffusion in membranes is the process through which gases are driven across a barrier due to concentration gradients, rather than pressure gradients. As with many processes, the rate of gas diffusing out of a membrane is be countered by a certain amount of gas diffusing in, depending on the concentration gradients involved. In this case, pure carbon dioxide is flowing into the tube and has the opportunity to diffuse out through the membrane wall into the stagnant atmosphere. However, the air outside the tube also has the ability to diffuse in through the membrane wall. Both of these processes are illustrated in Figure A-1.

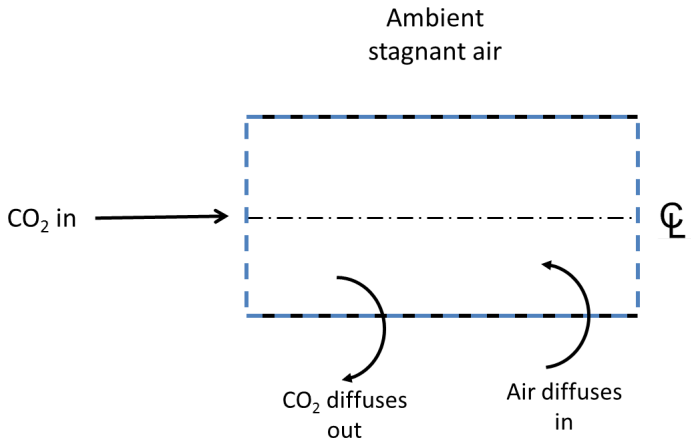

Figure A-1. Diffusion processes in a membrane tube

As presented by O'Hayre et al. (2009) the diffusive flux J'' can be determined by:

$$J'' = -D_{eff}\frac{c_1 - c_2}{t} \tag{A–1}$$

where D_{eff} is the effective diffusivity of the membrane and c_1 and c_2 are molar concentrations outside and inside the tube. The molar concentrations can be calculated using the ideal gas law:

$$c_i = \frac{p_i}{R_u T} \tag{A–2}$$

where p_i is the partial pressure of the gas, R_u is the universal gas constant, and T is the temperature. Considering that CO_2 makes up a relatively small fraction of the atmospheric gas, a large CO_2 concentration difference is expected between the inside and outside of the tube. However, since the concentration of air inside the tube is also very low, there is a large concentration difference in the opposite direction. Since this study is concerned with the net flux through the tube walls, if these two diffusion rates are similar, then the net diffusion will be negligible and pressure-driven flow, governed by Darcy's Law, will be the only significant driver.

Using Equation A–1, the net flux can be expressed as:

$$J''_{net} = J''_{CO_2} + J''_{air} \tag{A–3}$$

$$J''_{net} = -D_{eff,CO_2,air}\frac{c_{out,CO_2} - c_{in,CO_2}}{t} - D_{eff,air,CO_2}\frac{c_{out,air} - c_{in,air}}{t} \tag{A–4}$$

O'Hayre et al. states that $D_{eff,i,j} = D_{eff,j,i}$ is equal for for any pair of gases. Therefore,

$$J''_{net} = -\frac{D_{eff}}{t}\left[(c_{out,CO_2} - c_{in,CO_2}) + (c_{out,air} - c_{in,air})\right] \tag{A–5}$$

Defining c_{atm} as the total concentration of the ambient air, c_{int} as the total concentration inside the membrane, and y_{CO_2} as the mole fraction of CO_2 in the atmosphere, Equation A–5 can be written as:

$$J''_{net} = -\frac{D_{eff}}{t}\left[(y_{CO_2}c_{atm} - c_{int,CO_2}) + ((1 - y_{CO_2})c_{atm} - c_{int,air})\right] \tag{A–6}$$

Assuming that, since the fraction of air in the CO_2 stream is very low, $c_{int,air}/c_{int,CO_2} \sim 0$, this can be written as:

$$J''_{net} = -\frac{D_{eff}}{t}\left[\left(y_{CO_2}\frac{c_{atm}}{c_{int,CO_2}} - \frac{c_{int,CO_2}}{c_{int,CO_2}}\right) + \left((1-y_{CO_2})\frac{c_{atm}}{c_{int,CO_2}} - \frac{c_{int,air}}{c_{int,CO_2}}\right)\right] \tag{A–7}$$

$$J''_{net} \sim -\frac{D_{eff}}{t}\left[(y_{CO_2}\frac{c_{atm}}{c_{int,CO_2}} - 1) + ((1-y_{CO_2})\frac{c_{atm}}{c_{int,CO_2}} - 0)\right] \tag{A–8}$$

Finally, since there is only a few inches of water in absolute pressure difference between the inside and outside of the membrane, $c_{atm}/c_{int,CO_2} \sim 1$, allowing Equation A–8 to be expressed as:

$$J''_{net} \sim -\frac{D_{eff}}{t}\left[(y_{CO_2} - 1) + (1-y_{CO_2})\right] = 0 \tag{A–9}$$

$$J''_{net} \sim 0 \tag{A–10}$$

Therefore, the net diffusive flux is negligible for this analysis.

APPENDIX B
DETERMINATION OF SKIN FRICTION COEFFICIENT FOR A POROUS TUBE

A method to determine the skin friction coefficient c_f for a porous tube is shown here using the method of Kinney (1968).

Assuming a fully developed flow, the similarity solution of Yuan and Finkelstein (1956) can be used. The axial velocity expressed in terms of the dimensionless stream function f is:

$$u = 2\overline{u} f'(\eta) \tag{B–1}$$

The axial momentum equation 1–3 can then be expressed as :

$$0 = \eta f''' + f'' - \frac{\lambda_D}{2}(f'^2 - f f'') + \frac{\Gamma}{16} \tag{B–2}$$

where $\xi = x/R$ and Γ is a dimensionless pressure drop, constant for fully-developed flow and defined as:

$$\Gamma = -\frac{Re_D}{\rho \overline{u}^2}\frac{\partial p}{\partial \xi} \tag{B–3}$$

Integrating Equation B–2 aross the tube cross section and applying boundary conditions, Γ can be expressed as:

$$\Gamma = -16 f''(1) + 16\lambda_D \int_0^1 f'^2 d\eta \tag{B–4}$$

The term $f''(1)$ can be rewritten using Equation B–1:

$$f''(1) = \frac{1}{2\overline{u}} \left[\frac{\partial u}{\partial \eta}\right]_{\eta=1} \tag{B–5}$$

$$= \frac{R}{4\overline{u}} \frac{\partial u}{\partial r} \tag{B–6}$$

$$= -\frac{Re_D}{8\rho\overline{u}^2} \left(-\mu \frac{\partial u}{\partial r}\right) \tag{B–7}$$

$$= -\frac{Re_D}{16} \left(\frac{\tau_w}{\frac{1}{2}\rho\overline{u}^2}\right) \tag{B–8}$$

$$= -\frac{Re_D c_f}{16} \tag{B–9}$$

Furthermore, the discrete integral in Equation B–4 will be a constant, as f is a function of η only. Therefore, Equation B–4 can be written as:

$$\Gamma = c_f Re_D + 16\lambda_D \times \text{constant} \tag{B–10}$$

Noting again that Γ is constant for fully-developed flow, Equation B–10 reveals that $c_f Re_D$ is strictly a function of λ_D. Raithby (1971) developed an empirical relationship for $c_f Re_D$ as a function of λ_D, which is shown in Equation 2–24.

REFERENCES

Bansal, J.L. “Laminar flow through a uniform circular pipe with small suction.” *Proceedings of the National Institute of Science of India* 32 (1966).4: 368–378.

Belfort, G. and Nagata, N. “Fluid mechanics and cross-flow filtration: some thoughts.” *Desalination* 53 (1985).1-3: 57–79.

Berman, A.S. “Laminar flow in channels with porous walls.” *Journal of Applied Physics* 24 (1953).9: 1232–1235.

———. “Concerning laminar flow in channels with porous walls.” *Journal of Applied Physics* 27 (1956).12: 1557–1558.

———. “Effects of porous boundaries on the flow of fluids in systems with various geometries.” *Proceedings of the Second U.N. International Conference on the Peaceful Uses of Atomic Energy*. 1958a.

———. “Laminar flow in an annulus with porous walls.” *Journal of Applied Physics* 29 (1958b).1: 71–75.

Brady, J.F. “Flow development in a porous channel and tube.” *Physics of Fluids* 27 (1984): 1061.

Bundy, R.D. and Weissberg, H.L. “Experimental study of fully developed laminar flow in a porous pipe with wall injection.” *Physics of Fluids* 13 (1970): 2613.

Chatterjee, S.G. and Belfort, G. “Fluid flow in an idealized spiral wound membrane module.” *Journal of membrane science* 28 (1986).2: 191–208.

Eckert, E.R.G. and Drake, R.M. *Heat and mass transfer*. R.E. Krieger Pub. Co., 1959.

Galowin, L.S., Fletcher, L.S., and DeSantis, M.J. “Investigation of laminar flow in a porous pipe with variable wall suction.” *American Institute of Aeronautics and Astronautics Thermophysics Conference 8 th Palm Springs Calif*. 1973.

Hornbeck, R.W., Rouleau, W.T., and Osterle, F. “Laminar entry problem in porous tubes.” *Physics of Fluids* 6 (1963): 1649.

Karode, Sandeep K. “Laminar flow in channels with porous wall, revisited.” *Journal of Membrane Science* 191 (2001): 237–241.

Kinney, R.B. “Fully developed frictional and heat-transfer characteristics of laminar flow in porous tubes.” *International Journal of Heat and Mass Transfer* 11 (1968).9: 1393–1401.

Lawson, Kevin W., Hall, Matthew S., and Lloyd, Douglas R. “Compaction of microporous membranes used in membrane distillation. I. Effect on gas permeability.” *Journal of Membrane Science* 101 (1995).1-2: 99–108.

Lawson, Kevin W. and Lloyd, Douglas R. “Membrane distillation.” *Journal of Membrane Science* 124 (1997): 1–25.

Majdalani, J. and Flandro, G.A. “The oscillatory pipe flow with arbitrary wall injection.” *Proceedings of the Royal Society of London. Series A: Mathematical, Physical and Engineering Sciences* 458 (2002).2023: 1621–1651.

Mason, E.A. and Malinauskas, A.P. *Gas Transport in Porous Media: The Dusty Gas Model*. Elsevier Amsterdam-Oxford-New York, 1983.

Mason, E.A., Malinauskas, A.P., and Evans III, R.B. “Flow and diffusion of gases in porous media.” *The Journal of Chemical Physics* 46 (1967): 3199.

McGuire, Kenneth S., Lawson, Kevin W., and Lloyd, Douglas R. “Pore size distribution determination from liquid permeation through microporous membranes.” *Journal of Membrane Science* 99 (1995): 127–137.

Mellis, Rainer, Gill, William N., and Georges, Belfort. “Fluid dynamics in a tubular membrane: theory and experiment.” *Chemical Engineering Communications* 122 (1993).1: 103–125.

Morduchow, M. “On laminar flow through a channel or tube with injection: application of method of averages.” *Quart. J. Appl. Math* 14 (1957).4: 361–368.

Moussy, Y. and Snider, AD. “Laminar flow over pipes with injection and suction through the porous wall at low Reynolds number.” *Journal of Membrane Science* 327 (2009).1-2: 104–107.

Mulder, M. *Basic principles of membrane technology*. Springer, 1996.

Munson-McGee, Stuart H. “An approximate analytical solution for the fluid dynamics of laminar flow in porous tube.” *Journal of Membrane Science* 197 (2002): 223–230.

O’Hayre, Ryan P., won Cha, Suk, Colella, Whitney G., and Prinz, Fritz B. *Fuel Cell Fundamentals*. John Wiley and Sons, 2009, second ed.

Oxarango, Laurent, Schmitz, Philippe, and Quintard, Michel. “Laminar flow in channels with wall suction or injection: a new model to study multi-channel filtration systems.” *Chemical Engineering Science* 59 (2004): 1039–1051.

Quaile, J.P. and Levy, E.K. “Laminar flow in a porous tube with suction.” *Journal of Heat Transfer* 97 (1975): 66.

Quaile, P. and Levy, E.K. “Pressure variations in an incompressible laminar tube flow with uniform suction.” *AIAA Paper* 72 (1972): 257.

Raithby, G. “Laminar heat transfer in the thermal entrance region of circular tubes and two-dimensional rectangular ducts with wall suction and injection.” *International Journal of Heat and Mass Transfer* 14 (1971).2: 223–243.

Sellars, J.R. “Laminar flow in channels with porous walls at high suction Reynolds numbers.” *Journal of Applied Physics* 26 (1955): 489.

Skalak, F.M. and Wang, C.Y. “Pulsatile flow in a tube with wall injection and suction.” *Applied Scientific Research* 33 (1977).3: 269–307.

Terrill, R.M. “An exact solution for flow in a porous pipe.” *Zeitschrift für Angewandte Mathematik und Physik (ZAMP)* 33 (1982).4: 547–552.

———. “Laminar flow in a porous tube.” *Journal of fluids engineering* 105 (1983): 303.

Terrill, R.M. and Thomas, P.W. “On laminar flow through a uniformly porous pipe.” *Applied Scientific Research* 21 (1969).1: 37–67.

Verma, P.D. and Bansal, J.L. “Flow of a viscous incompressible fluid between two parallel plates, one in uniform motion and the other at rest with uniform suction at the stationary plate.” *Proceedings of the Indian Academy of Sciences* 64 (1966): 385–396.

Weissberg, H.L. “Laminar flow in the entrance region of a porous pipe.” *Physics of Fluids* 2 (1959): 510.

White Jr, F.M. “Laminar flow in a uniformly porous tube.” *Journal of Applied Mechanics* 29 (1962): 201.

Yuan, S.W. “Further investigation of laminar flow in channels with porous walls.” *Journal of Applied Physics* 27 (1956): 267–269.

Yuan, S.W. and Finkelstein, A.B. “Laminar pipe flow with injection and suction through a porous wall.” *Transactions of the ASME* 78 (1956): 719–724.

BIOGRAPHICAL SKETCH

Aaron Robert Meles was born

. He graduated from .

Attending Rose-Hulman Institute of Technology (Terre Haute, Indiana), he earned his bachelor's degree in 2008, majoring in mechanical engineering (with a concentration in aerospace engineering) and minoring in English language and literature. While at Rose-Hulman, Aaron secured a 4.0 GPA while at the same time serving as the Vice President of Tau Beta Pi (engineering honor society), Vice President of the Rose Drama Club, and Editor-in-Chief of the Rose Thorn, the student newspaper. Upon graduation, Aaron began work at Power Systems, Mfg. (Jupiter, Florida) as an aerothermal engineer, specializing in industrial gas turbine combustion and tuning. In August 2010, he began pursuing his master's degree in mechanical engineering at the University of North Florida (Jacksonville, Florida), where his graduate research involved developing a portable direct methanol fuel cell system for small electronics. Upon graduation in 2012, Aaron plans to return to Power Systems, Mfg. as an aerothermal engineer.